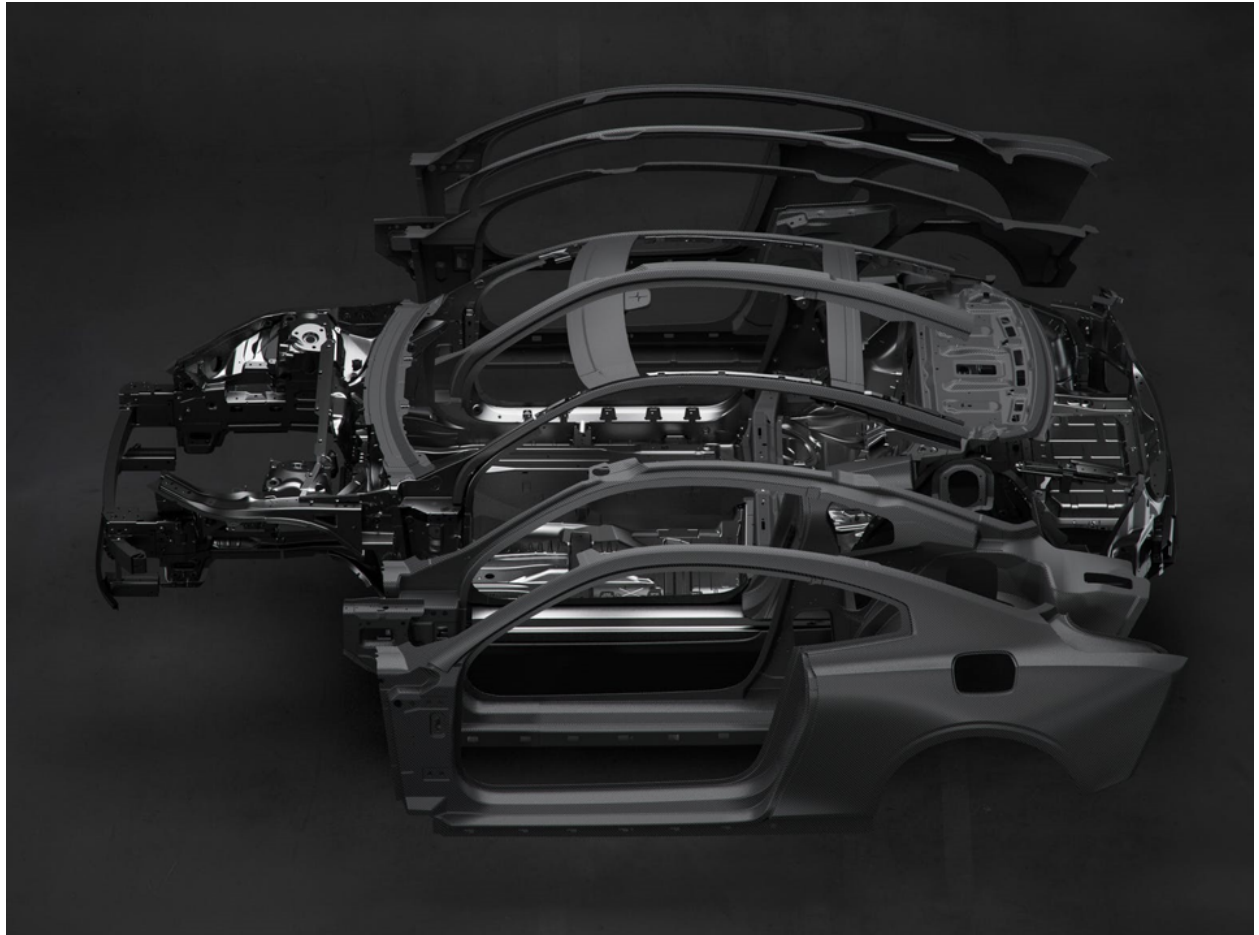




CHALMERS



Virtual Durability Testing of CFRP materials

Master Thesis in Applied Mechanics

Authors

KEVIN STÅHL
ANTON ANDERSSON

Supervisor

Renaud Gutkin

Virtual Durability Testing of CFRP materials
Master Thesis in Applied Mechanics
KEVIN STÅHL
ANTON ANDERSSON

© KEVIN STÅHL, 2019
© ANTON ANDERSSON, 2019

Department of industrial and materials science
Chalmers University of Technology
SE-412 96 Gothenburg
Sweden
Telefon: +46 (0)31 772 1000

Cover:
Explosion chart of the Polestar 1 car body, one of the projects that would benefit from this research.

Department of industrial and materials science
Gothenburg, Sweden 2019

Acknowledgement

A special thank to Renaud Gutin, that in his role as supervisor has contributed with much knowledge, guidance and support throughout this project. Also, we would like to show our gratitude to Henrik Molker who has contributed with his knowledge in NCF fabrics among others. Prof. Leif Asp has as the examiner of this project supported with additional guidance and has continuously emphasized the importance of our learning, for which we are grateful for.

Our gratitude goes towards Volvo Cars for providing us with workspace, computers, softwares and experiments, all vital components for the progress of this project.

A final thanks goes to all the colleagues at Volvo Cars, who have included us in their group and created a friendly work environment.

Authors, Gothenburg, May 2019

Virtual Durability Testing of CFRP materials
KEVIN STÅHL
ANTON ANDERSSON
Department of industrial and materials science
Chalmers University of Technology

Abstract

The demand for products made from carbon fibre reinforced polymers (CFRP) is rapidly increasing. As in the car industry where there is a need for more lightweight and energy efficient solutions to lower the environmental effects. The new Polestar 1 car is an example where CFRP has been introduced in several parts of the car body. When usage increases, it also becomes more important to understand the properties of the material. To lower the costs of material tests, this project has developed a test methodology detailing the way to perform virtual material tests at Volvo Cars.

The first part of the project covers unidirectional (UD) plies which are stacked together into laminates with fibre orientations at different angles. A 3D physically based constitutive material model, called LaRC05 which was developed by Pinho, Iannucci, and Robinson (2006a), is used in the project. This model proved to be one of the more accurate material models during the second World Wide Failure Exercise (Kaddour and Hinton, 2013). Later in the project, a strategy to model more complex fibre architectures and to transform the model into different test environments is proposed.

The developed methodology reduces the number of physical laminate tests and shows good correlation towards physical tests in room temperature environment. It can predict the strength at first sign of failure and models the same failure mode that can be seen in physical tests. Further work has to be performed on how to predict failure in hot and wet test environments. For cold environments it is recommended to look closer on compression tests while tension tests show a good correlation. Weak areas of the methodology are discussed together with possible actions of improvement.

Keywords: CFRP, Virtual analysis, T700, NCF, Twill, Abaqus, Finite element, Composite failure, Test methodology

Abbreviations

CFRP	Carbon Fibre Reinforced Polymers
UD	Unidirectional
NCF	Non-Crimp Fabric
FE	Finite Element
BC	Boundary Condition
WWFE	World Wide Failure Exercise
UNT	Unnotched Tension
UNC	Unnotched Compression
OHT	Open Hole Tension
OHC	Open Hole Compression
RTD	Room Temperature Dry
HTW	Hot Temperature Wet
CTD	Cold Temperature Dry
VT	Virtual Test
FT	Fibre Tension
FK	Fibre Kinking
MT	Matrix Tension
MC	Matrix Compression
MS	Matrix Shear

Contents

1	Introduction	1
2	Theory	3
2.1	Material model	3
2.1.1	Fibre tensile failure	3
2.1.2	Matrix tensile failure	3
2.1.3	Matrix compression failure	4
2.1.4	Fibre-kinking failure, longitudinal compressive failure	5
2.1.5	Damage propagation	6
2.1.6	In-situ strength	7
2.2	Mesh resolution	7
2.3	Non-UD fibre architectures	7
2.3.1	Twill	7
2.3.2	NCF	9
2.4	Environmental effects on CFRP	9
3	Methodology	10
3.1	Project strategy	10
3.2	Finite Element Model	11
3.2.1	Boundary conditions	11
3.2.2	Contact condition	12
3.2.3	Mesh	13
3.3	Modelling technique for twill & NCF	14
3.4	Calibration of material parameters	15
3.4.1	UD-ply	15
3.4.2	Twill & NCF	17
3.4.3	Laminates	18
3.5	Environmental effects on CFRP	18
4	Correlation and validation of test procedure	20
4.1	Correlation UD-model	20
4.2	Correlation twill/NCF-model	24
4.3	Correlation environmental effects	29
5	Test procedure of new CFRP-materials	31
6	Discussion	32
6.1	Delamination	32
6.2	In-situ strength	33
6.3	Stiffness	33
6.4	Kink band prediction	34
6.5	Transverse fibre kinking	34
6.6	Nonlinear shear	36
6.7	Environmental effects on CFRP	37

6.8	Additional error sources	37
7	Conclusions and Future work	38
	Appendices	I
A	Calibrated material data	I
B	User guide for virtual material testing	II
B.1	Building the FE-model	II
B.2	Collect material data	V
B.3	Calibrate collected material data	VIII
B.4	In-situ strength	VIII
B.5	Different environments	IX
C	Stress-strain charts for all unnotched laminate tests	X

1 Introduction

This master thesis deals with virtual material testing of carbon fibre reinforced polymers (CFRP) at Volvo Cars. The applications for carbon fibre composites are increasing rapidly as there is a need for more energy efficient solutions within the car industry today. Producing parts made from CFRP makes it possible to save weight while keeping stiffness and strength high. When usage increases it becomes more important to understand the properties of the material. For new cars e.g. the Polestar 1, there is a need to ensure the structural robustness of the car body and other components that are manufactured in CFRP.

Investigating the durability of CFRP is both difficult and expensive. Virtual material tests will have an important role to lower the costs when an increased number of specimens have to be tested. By working with virtual tests, the total cost for material tests could be reduced to less than 10%. Furthermore, the ability to perform virtual tests will shorten the lead times with a similar factor during development (Gardiner, 2017).

There has been a lot of research in the area of CFRP modelling over the years but most material models are still quite inaccurate in predicting failure of CFRP. This became obvious after the second World Wide Failure Exercise (WWFE-II) which compared the failure prediction of several different material models (Kaddour and Hinton, 2013).

A material model that was proposed by Pinho et al. (2006a) will be used as a foundation for this project. This model has previously been used for correlation work in several different projects, for example by Chen, Tay, Biaz, and Pinho (2012) who applied the model on the material IM7/8552. The performance of this model was also emphasised in the WWFE-II and has shown good correlation when compared with experimental data.

With the background given above, the objective of this project is to answer the following question.

- By using a reduced number of physical tests, is it possible to predict strength for unnotched and open hole tests in tension and compression for different laminates, hole diameters and environments?

If the virtual tests are successful, the outcome will be a detailed methodology for virtual material testing of CFRP. This methodology will be used to identify material strength which are to be used for product development in future Volvo Cars projects containing CFRP. The virtual simulation can be considered successful if it accurately can predict the mode of failure. Further, a trend concerning strength and stiffness should be seen, relating the virtual tests to the physical ones. If the correlations between all virtual and physical tests are within 15% it can be assessed as a good result.

1. Introduction

The analyses in this project are focused on three different laminates named A, B and C, defined in *Table 1.1*. Three different fabric types, unidirectional (UD) plies, twill plies and plies of Non-Crimp fabric (NCF) have been used to build these laminates. All composites are made from carbon fibres of type T700 with an epoxy matrix. Some virtual tests of carbon-epoxy IM7-8552 are also performed.

Table 1.1: Laminate composition used in the project.

	Thickness [mm]	Laminate A	Laminate B	Laminate C
UD	0.30	6	0	0
Twill	0.65	4	4	2
NCF	0.3	0	2	2
Layup*		$[\pm 45^T, 0, 0, \pm 45^T, 0]_S$	$[\pm 45^N, (0/90)^T, \pm 45^T]_S$	$[\pm 45^N, (0/90)^T]_S$

*Notation ± 45 or $0/90$ represents one layer of twill or NCF. Superscript T represents twill and superscript N represents NCF.

The physical tests used in this thesis are summarized in *Figure 1.1*. They consists of unnotched tension (UNT), unnotched compression (UNC), open hole tension (OHT), open hole compression (OHC) tests with different load directions. The laminates in *Table 1.1* are tested as well as the fabrics from which the laminates were built. Shear tests at material level have also been performed.

		T700-DT120			LAMINATES TESTED							
RTD - Room Temperature	LOAD	Twill	UD	NCF	LAMINATE A			LAMINATE B		LAMINATE C		
		0°	0°	90°	0°	45°	90°	0°	45°	0°	45°	
RTD - Room Temperature	TENSION	X	X	X	X	X	X	X	X	X	X	UNT
					X	X	X	X	X	X	X	OHT
	COMPRESSION	X	X	X	X	X	X	X	X	X	X	UNC
					X	X	X	X	X	X	X	OHC
	SHEAR	X	X	X								
		T700-DT120			LAMINATES TESTED							
HTW - Hot / Wet +80	LOAD	Twill	UD	NCF	LAMINATE A			LAMINATE B		LAMINATE C		
		0°	0°	90°	0°	45°	90°	0°	45°	0°	45°	
HTW - Hot / Wet +80	TENSION				X	X		X	X			UNT
					X	X		X	X			OHT
	COMPRESSION		X	X	X	X		X	X			UNC
					X	X		X	X			OHC
	SHEAR		X									
		T700-DT120			LAMINATES TESTED							
CTD - Cold / Dry -40	LOAD	Twill	UD	NCF	LAMINATE A			LAMINATE B		LAMINATE C		
		0°	0°	90°	0°	45°	90°	0°	45°	0°	45°	
CTD - Cold / Dry -40	TENSION				X	X		X	X			UNT
					X	X		X	X			OHT
	COMPRESSION		X	X	X	X		X	X			UNC
					X	X		X	X			OHC
	SHEAR		X									

Figure 1.1: Physical tests performed by Volvo Cars. See *Table 1.1* for laminate details.

2 Theory

This chapter covers the main part of the theory that has been used in this project. The first section is an introduction to the material model. This is a necessary part to understand in order to make any conclusions from the virtual tests. The chapter will later deal with theories about different fibre architectures and the behaviour of CFRP in different environments. These theories will all have a major impact on the development of a test methodology.

2.1 Material model

A good material model is vital in order to develop a test methodology that achieves good correlation between physical and virtual tests. The material model that was implemented in this project is called LaRC05. The model was proposed by Pinho et al. (2006a) and handles the failure equations of four different failure modes. The failure model states equations to calculate f_i , which is the failure index. A ply has failed when f_i becomes equal to one in any mode.

When failure has initialized, the extent of damage, d , starts to grow from zero to one, where complete failure has occurred. Equation 2.1 describes how the effective stress for a failed element is replaced with the reduced damage stress. This section presents the theory behind each one of these and the following damage evolution.

$$\sigma \leftarrow (1 - d)\sigma \quad (2.1)$$

2.1.1 Fibre tensile failure

During longitudinal tensile loading of a composite, failure will initiate as a result of fibre breakage due to high longitudinal stresses. The failure of fibres during tensile loading is predicted from the longitudinal stress (σ_1) alone, see equation 2.2 where X_t is the longitudinal tensile strength. From experimental data it has been concluded that there is no influence from transverse or shear stresses. (Pinho et al., 2006a)

$$f_{ft} = \frac{\sigma_1}{X_t} \quad (2.2)$$

2.1.2 Matrix tensile failure

If a CFRP-ply is loaded in tension transverse to the fibre orientation, failure will result from microcracking. From the World Wide Failure Exercise (WWFE), it was possible to form a quadratic expression between the transverse tensile stress and the shear stress components, see equation 2.3 (Pinho et al., 2006a). The transverse tensile strength is denoted Y_t , the in-plane and out-of-plane shear strengths are S_{12} and S_{13} , respectively.

$$f_{mt} = \left(\frac{\sigma_n}{Y_t}\right)^2 + \left(\frac{\tau_{13}}{S_{13}}\right)^2 + \left(\frac{\tau_{12}}{S_{12}}\right)^2 \quad (2.3)$$

2.1.3 Matrix compression failure

Matrix failure during transverse compression of a composite is driven by shear. Hence, the fracture plane should be oriented at an angle $\alpha_0 = 45^\circ$ with the out of plane direction. From experiments it has been shown that this angle rather tends to be $\alpha_0 \approx 53^\circ$. The reason for this is friction occurring in matrix micro-cracks. The friction reduces the sliding between crack surfaces and thus increases the load that can be applied before failure.

The failure index is predicted from stresses acting on the fracture plane. Pinho, Iannucci, and Robinsson (2006b) describes the implementation of the material model into an FE-code. The fracture plane angle is found by rotating applied stresses into a number of possible fracture angles between 0° and 180° . The failure index is then calculated as in equation 2.4 and the most likely fracture plane is the one where the failure index takes its largest value. Here μ_T and μ_L are the strength slope coefficients. These will increase the strength due to friction under compressive loads. A potential fracture plane with stress definitions are shown in *Figure 2.1*.

$$f_{mc} = \left(\frac{\tau_{13}}{S_{13} - \mu_T \sigma_n} \right)^2 + \left(\frac{\tau_{12}}{S_{12} - \mu_L \sigma_n} \right)^2 \quad (2.4)$$

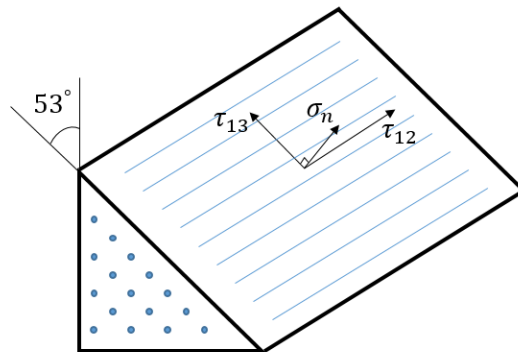


Figure 2.1: Stresses acting on a potential fracture plane for matrix compression failure.

2.1.4 Fibre-kinking failure, longitudinal compressive failure

The last failure mode that is accounted for in the material model is fibre kinking. This compressive failure mode is driven from an imperfection, modelled as a fibre misalignment angle ϕ explained in *Figure 2.2*. The model proposed by Pinho et al. (2006a) assumes that there is an initial misalignment angle (ϕ_0) in all plies. The angle will increase when the ply is subjected to compressive loads, resulting in a rotating motion in the kinked cross section. This rotation will increase the shear stresses in the matrix within this area. The result of this is that the same criterion that was used to model compressive strength of the matrix (equation 2.4) can be implemented to assess failure in fibre kinking. Since experiments have shown that fibre kinking is a three dimensional behaviour, Pinho et al. (2006a) also introduces the angle ψ , seen in *Figure 2.3*. This is the angle between the laminate plane and the misalignment frame and it is varied between 0 and π to find the kink plane. The stresses in *Figure 2.2* must be transformed into material orientation in order to be implemented in equation 2.4. Equation 2.5 is used to rotate the stresses at an angle ψ around axis 1.

$$\begin{aligned}
\sigma_{2\psi} &= \frac{\sigma_2 + \sigma_3}{2} + \frac{\sigma_2 - \sigma_3}{2} \cos 2\psi + \tau_{23} \sin 2\psi \\
\sigma_{3\psi} &= \sigma_2 + \sigma_3 - \sigma_{2\psi} \\
\tau_{12\psi} &= \tau_{12} \cos \psi + \tau_{31} \sin \psi \\
\tau_{2\psi 3\psi} &= -\frac{\sigma_2 - \sigma_3}{2} \sin 2\psi + \tau_{23} \cos 2\psi \\
\tau_{3\psi 1} &= \tau_{31} \cos \psi - \tau_{12} \sin \psi
\end{aligned} \tag{2.5}$$

When stresses are rotated into the misalignment frame they can be further rotated into the fibre misalignment angle ϕ . This is done by equation 2.6.

$$\begin{aligned}
\sigma_{1m} &= \frac{\sigma_1 + \sigma_{2\psi}}{2} + \frac{\sigma_1 - \sigma_{2\psi}}{2} \cos 2\phi + \tau_{12\psi} \sin 2\phi \\
\sigma_{2m} &= \sigma_1 + \sigma_{2\psi} - \sigma_{1m} \\
\tau_{1m 2m} &= -\frac{\sigma_1 - \sigma_{2\psi}}{2} \sin 2\phi + \tau_{12\psi} \cos 2\phi \\
\tau_{2m 3\psi} &= \tau_{2\psi 3\psi} \cos \phi - \tau_{3\psi 1} \sin \phi \\
\tau_{3\psi 1m} &= \tau_{3\psi 1} \cos \phi
\end{aligned} \tag{2.6}$$

Finally the stresses acting on the fracture plane used in equation 2.4 is found from equation 2.7 where α_0 is the fracture plane angle.

$$\begin{aligned}
\sigma_n &= \frac{\sigma_{2m} + \sigma_{3\psi}}{2} + \frac{\sigma_{2m} - \sigma_{3\psi}}{2} \cos 2\alpha_0 + \tau_{2m 3\psi} \sin 2\alpha_0 \\
\tau_{12} &= \tau_{1m 2m} \cos \alpha_0 + \tau_{3\psi 1m} \sin \alpha_0 \\
\tau_{13} &= -\frac{\sigma_{2m} - \sigma_{3\psi}}{2} \sin 2\alpha_0 + \tau_{2m 3\psi} \cos 2\alpha_0
\end{aligned} \tag{2.7}$$

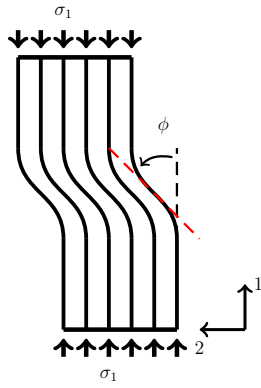


Figure 2.2: Fibre misalignment during compression, 2D.

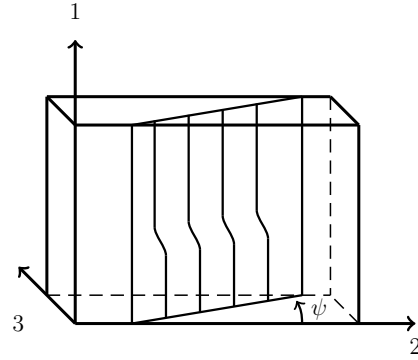


Figure 2.3: Fibre misalignment during compression, 3D.

The initial misalignment angle will have a large impact on the compressive strength of a laminate and need to be calibrated in order to fit experimental tests. Equation 2.8 proposed by Argon (1972), relating the compressive failure stress and the longitudinal shear failure stress to the initial misalignment angle, can serve as a benchmark for calibration.

$$X_c = \frac{S_{12}}{\phi_0} \quad (2.8)$$

2.1.5 Damage propagation

Once failure has occurred, damage starts to propagate through the material. The damage will cause linear softening of the material as shown in *Figure 2.4*. The slope of the linear softening is decided from the critical energy release rate G_C and the element length l_e for a specific failure mode. Hence, the critical energy release rate has to be measured and work as an input to the material model.

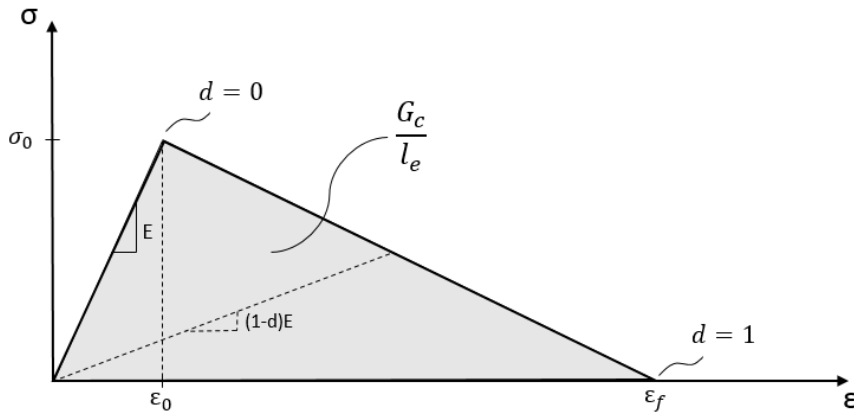


Figure 2.4: Stress-strain curve showing the bilinear constitutive law of the material with the damage variable d .

2.1.6 In-situ strength

In-situ strength described by Camanho, Dávila, Pinho, Iannucci, and Robinson (2006) is a phenomenon that increases the transverse tensile strength and shear strengths of a ply if it is a part of a laminate. A ply will have different strength depending on whether it is an outer ply or is embedded in the laminate. Also ply thickness and the amount of plies with the same angle that are stacked upon each other will affect the in-situ strength. In-situ strength is not implemented in the material model from Pinho et al. (2006a) but will be considered in this project.

2.2 Mesh resolution

The mesh dependency of a FE-model is a well studied field. Generally a finer mesh will result in a more accurate solution. But above this, there is a particular requirement on element size concerning damage propagation. In order to capture the damage propagation for a particular failure mode it follows that $\varepsilon_f > \varepsilon_0$. The relation in equation 2.9 can be derived from *Figure 2.4*. By using equation 2.9 it is possible to calculate the critical element length l_e^* when $\varepsilon_f = \varepsilon_0$ for each failure mode as in equation 2.10.

$$\frac{G_c}{l_e} = \frac{\sigma_0 \cdot \varepsilon_f}{2} \quad (2.9)$$

$$l_e^* = \frac{2E \cdot G_c}{\sigma_0^2} \quad (2.10)$$

2.3 Non-UD fibre architectures

The laminates that will be analysed in the later stage of this project have plies of different orientations merged together either by weaving or stitching. These require some consideration when modelled compared to the UD-ply. This section gives an introduction to the new mechanics that need to be accounted for when modelling these materials. It covers the two different non-UD fibre architectures found in this project, twill and NCF. The theory covered in this section is described by Greenhalgh (2009).

2.3.1 Twill

The twill material is constructed through bundles of fibres weft together into a cloth like structure, seen in *Figure 2.6*. This gives the material similar longitudinal and transverse characteristics. This fibre structure introduces new mechanisms in the fabric when loaded.

It has been observed that the first sign of failure in tension can be found in intralaminar matrix cracking or splits. The splits can then become an initiation site for fibre failure. Something to consider in weave materials is what in this report will be called matrix entrapment. A matrix crack will strive to grow along the fibres but the fibre pattern in the weave will force the crack to change direction, seen in *Figure 2.5*. Crossing fibre bundles will also make it more difficult for a matrix crack within the bundles to open. This will slow down the process and increase the fracture toughness.



Figure 2.5: Twill in which the matrix crack has changed direction at crossing fibre bundles during propagation.

The weaving introduces a lot of crimp on the fibres which reduces the strength of the fibres in the load carrying direction. This is more present during compressive loading due to an increased risk for fibre kinking. The compressive failure of a weave will often grow along a crimp line due to the local deformation.

Another mechanism that is provided by the weaving is a reduced risk of interlaminar delaminations. This behaviour comes from resin rich areas of the weave. The extra resin increases the ductility and fracture toughness in the seam to another ply. The undulation of a weave will make the fracture surface less smooth and thus increase fracture toughness further. The delamination behaviour is particularly difficult to model since it grows segment wise and will be halted by crossing fibres or resin rich areas.

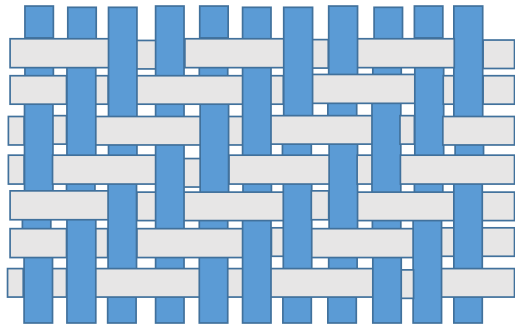


Figure 2.6: The weave sequence of a Twill material.

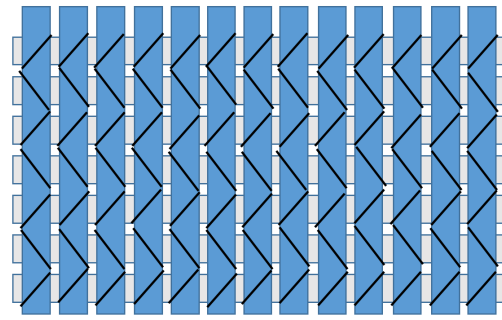


Figure 2.7: The weave sequence of a NCF material.

2.3.2 NCF

The NCF (Non-crimp fabric) is a material where plies consisting of fibre bundles are stitched together, see *Figure 2.7*. The idea is to reduce the crimp that occurs in woven materials such as the twill and hence get better mechanical properties. However, the stitches will induce some crimp and also some damage into the material.

When loaded in tension, transverse cracking within the bundles or at the interfaces between fibre rich bundles and resin rich regions are likely to be the first failure event. As a consequence of transverse cracks, delamination will initiate at the bundles. Although delamination can occur it is generally not the critical failure mechanism in NCF materials. In compression loading, the NCF material usually fails due to fibre kinking where the crimp has a significant effect on the strength.

2.4 Environmental effects on CFRP

When a material is subjected to different environmental conditions such as heat or moisture, its properties will change. For a CFRP, the fibre properties and the matrix properties will not change in the same way if heated or soaked. This means that depending on the applied load and failure mode, the composite properties will also change differently.

Well known is that heat will make polymeric material less stiff and more ductile. In the same way, cold temperatures will make a polymeric material stiffer and more brittle. For a polymer that is subjected to moisture, the glass transition temperature, T_g , will decrease. This means that heat effects will be present at a lower temperature than for a dry material.

Carbon fibres are not very sensitive to temperature or humidity which means that environmental effects on the fibre properties in most cases can be neglected. However, the load carrying capacity for a UD-composite loaded along the fibres can be significantly affected. This is due to the fact that the matrix capacity to transfer load between fibres will decrease in an environment with high temperature and humidity (Wang, Young, and Smith, 2011).

3 Methodology

This chapter covers the working procedure for the project and the developed test methodology. Several of different assumptions and strategies have been investigated during the development of the test methodology. However, all of them are not mentioned in this chapter. Instead, focus is on the methodology which turned out to be most accurate in predicting failure.

3.1 Project strategy

To find the best possible methodology for performing virtual material testing of CFRP it was important with a clear working procedure. *Figure 3.1* describes the procedure to develop the final methodology in three steps.

In the first step, a finite element model is developed. Different boundary conditions, contact conditions and mesh resolutions are evaluated. The FE-model is validated together with the material model towards physical tests on UD-laminates of material IM7/8552.

A second step starts when the FE-model together with the material model is validated for UD-laminates. This step includes development of a modelling technique for twill and NCF materials. The model is validated towards physical laminate tests performed by Volvo Cars, see *Figure 1.1*. This step also includes calibration of material parameters for T700/epoxy.

Finally the development of a model to perform virtual tests in other environments than room temperature is addressed. This model is also validated towards physical laminate tests from Volvo Cars.

This chapter covers the the outcome from these three steps and motivations for the choices that were made. The final methodology has been implemented in a PYTHON script so that input files can be generated quickly and with consistency. All virtual tests were run through ABAQUS Explicit.

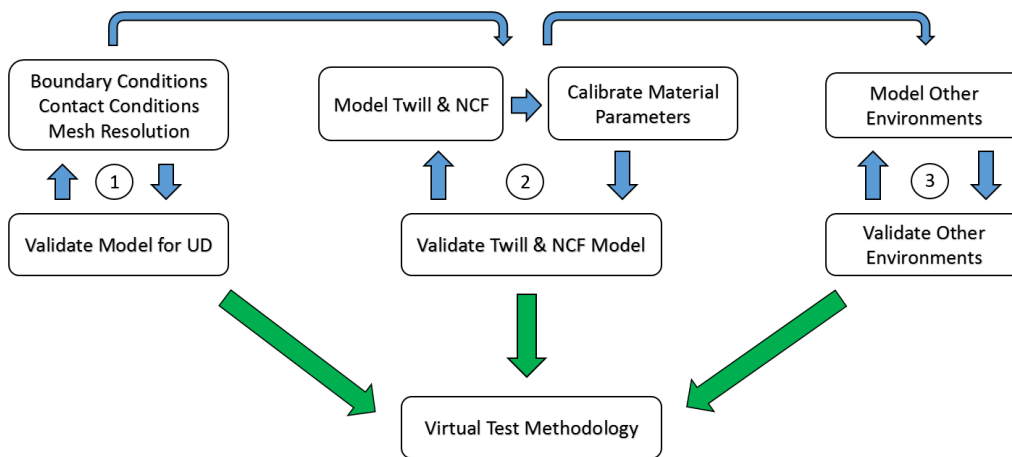


Figure 3.1: Flow chart visualizing the strategy for development of the test methodology.

3.2 Finite Element Model

This project aimed to develop a method that predicts failure in CFRP-laminates based on the material T700/epoxy. A first step to reach that goal was to develop an FE-model that together with the material model correlates well with physical tests of UD-laminates. Evaluation of the FE-model was done with a different material where the amount of available test data and research was higher. The CFRP-material chosen was IM7/8552 with research by Wisnom, Hallett, and Soutis (2010) among others. The material parameters used can be found in *Table A.1* and were retrieved from previous works in McElroy, Gutkin, and Pankow (2017).

The size of a coupon, especially width and thickness, can affect for example the delamination process, crack propagation and hence the resulting strength of a laminate (Wisnom et al., 2010). The virtual test coupons should therefore be modelled with the same size as the physical test coupons.

3.2.1 Boundary conditions

The measured strength of a CFRP material can be very sensitive to the test procedure. There are different standards to ensure reliability in the measured results. The experimental data in this project have been tested using standards from ASTM, seen in *Table 3.1*. The boundary conditions in the FE-model should mimic these standards as close as possible.

To accurately model the clamping of a coupon is difficult. The boundary conditions should simulate the clamping behaviour without inducing unrealistic stress concentrations at the end tabs. As in the physical tests, failure should occur close to the centre section of the coupon. To model this, 2.5 mm wide zones where failure cannot initiate are created at the ends of the test coupon, see *Figure 3.2*.

Two different combinations of boundary conditions were used in this project, one for tension and one for compression, see *Figure 3.2*. The tensile boundary condition uses a symmetry plane which reduces the number of elements. This works for tension tests but for compression tests the symmetry plane were found to prevent the formation of kink bands in out-of-plane directions. Hence, no symmetry plane was used to model compression tests.

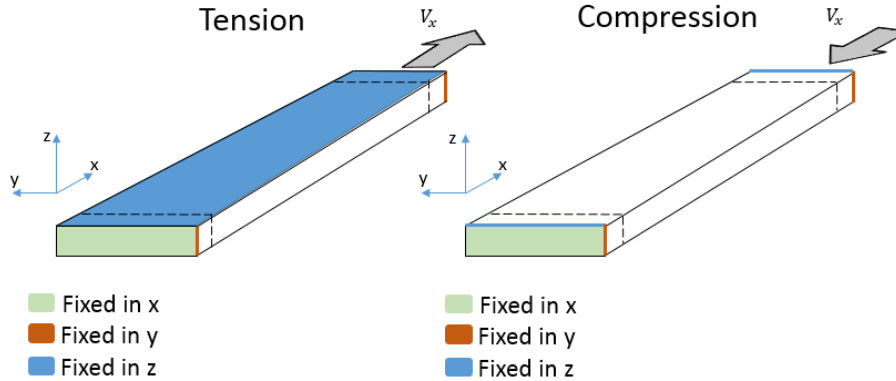


Figure 3.2: Boundary conditions used in the FE-model.

Table 3.1: Material properties that are extracted from physical tests.

	0°	90°	ASTM standard
Tension	E_1, X_t, ν_{12}	E_2, Y_t	ASTM D3039 (ASTM, 2017)
Compression	X_c	Y_c	ASTM D6641 (ASTM, 2016)
Shear	G_{12}, S_{12}		ASTM D5379 (ASTM, 2012)

3.2.2 Contact condition

The FE-model was created in such a way that each ply was modelled as a separate property, see *Figure 3.3*, with a material orientation defined from the layup. Each ply is one element high and nodes are shared between two plies next to each other if they have the same material orientation. Nodes are not shared if two plies next to each other have different material orientations. In such case, one node was created for each ply, see *Figure 3.4*. This allows delamination to form between plies of different material orientation but not between plies with the same material orientation. A contact condition was defined to bind plies of different orientation together. The contact was modelled with a traction separation law with damage propagation similar to damage model in the material model from Pinho et al. (2006a), see *Figure 2.4*. The properties of this contact are similar as the properties of the resin as suggested by Chen et al. (2012). These conditions may be subject to calibration depending on how well the behaviour of the virtual tests match experiments.

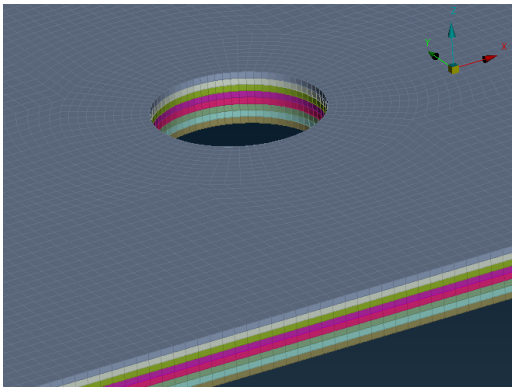


Figure 3.3: Model of a laminate where each layer has a separate property.

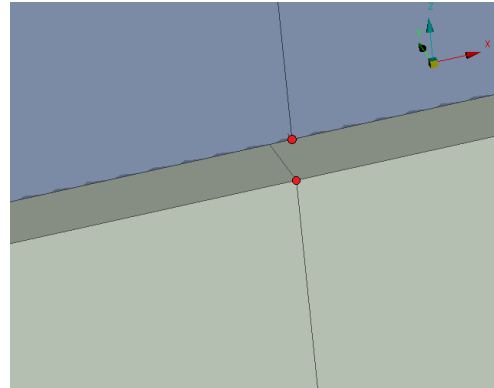


Figure 3.4: Plies of different orientations with one node for each layer.

3.2.3 Mesh

To find an approximate value of the critical element length for each failure mode, equation 2.10 was used. Results can be seen in *Table 3.2*. A mesh convergence study was then performed around the element length 0.3 mm, where the critical element length was expected to be. Based on the results of the mesh convergence study, see *Figure 3.5*, an element size of 0.25 mm was used throughout the project. According to equation 2.10 this element size is small enough for all materials studied in this project.

A smeared crack model is used to predict the crack propagation. This model distributes the stress concentrations at the crack tip over the element size. However, this continuum damage assumption becomes invalid if the element size is small enough to resolve the cracks.

The specimen used in the mesh convergence study was chosen to be a notched coupon with a hole diameter of 3.2 mm. The layup sequence was chosen as the simplest possible from Wisnom et al. (2010) ($[45/90/-45/0]_S$) in order to keep simulation times down. Further, the crack propagation process is more obvious in an open hole test due stress concentrations, which was therefore used in the study.

Table 3.2: Critical element length for IM7/8552 (with in-situ strength) for fibre tension, fibre kinking, matrix tension, matrix compression and matrix shear.

	FT	FK	MT	MC	MS	
σ_0	2340	1590	129	200	92.8	MPa
G_c	97.8	106	0.277	0.787	0.787	kJ/m ²
E	171000	171000	9080	9080	5290	MPa
l_e^*	6.1	14.4	0.3	0.36	0.97	mm

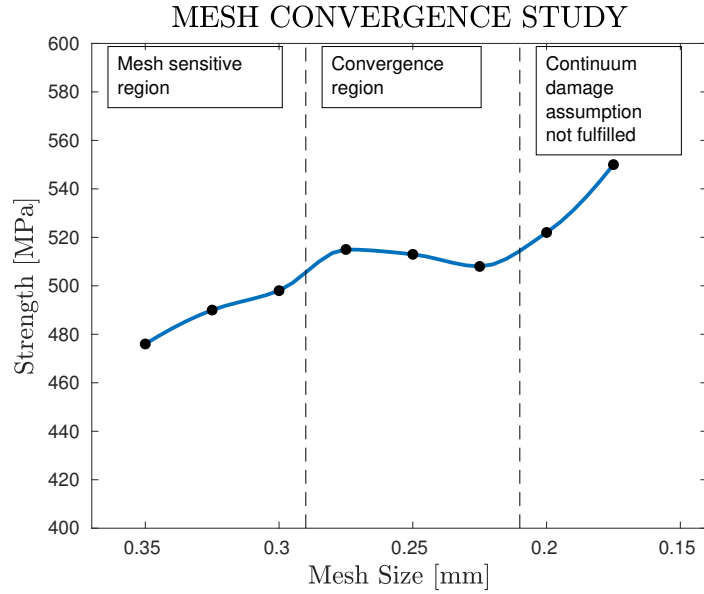


Figure 3.5: Mesh convergence for a IM7/8552 open hole laminate with layup $[45/90/-45/0]_S$ and hole diameter 3.2 mm.

3.3 Modelling technique for twill & NCF

When modelling twill and NCF, the available data from physical tests cannot be used as it is in the material model. This is since the material model is developed to work for UD-ply and has not been tested on other fabric architectures. Due to this it was decided to model the twill and NCF as two perpendicular UD-ply stacked upon each other. The mechanical properties of these ply are adjusted such that the combined properties of the $[0/90]$ UD-laminate match the properties of the fabric.

Other factors that have to be taken into account is the waviness/crimp of the fibres in different fabrics and the delamination properties within the twill and NCF respectively. A summary of differences between the fabrics that has been accounted for can be seen in *Table 3.3*.

Table 3.3: Mechanisms to capture for the different fabrics.

	Crimp	Matrix entrapment	Delamination intra-blanket
UD	Low	No	-
Twill	High	Yes	No
NCF (weak thread)	Medium	No	Yes
NCF (strong thread)	Medium	No	No

A bilinear damage law, see *Figure 3.6*, was used to model the matrix damage and energy release rate of the twill. This will make it possible to calibrate the second energy release rates such that the matrix entrapment is simulated correctly (Gutkin, Laffan, Pinho, Robinsson, and Curtis, 2011). The material model allows this modelling technique without any further development of the model. Further, no major delaminations can occur inside a twill. It was therefore decided to use an unbreakable contact within a twill.

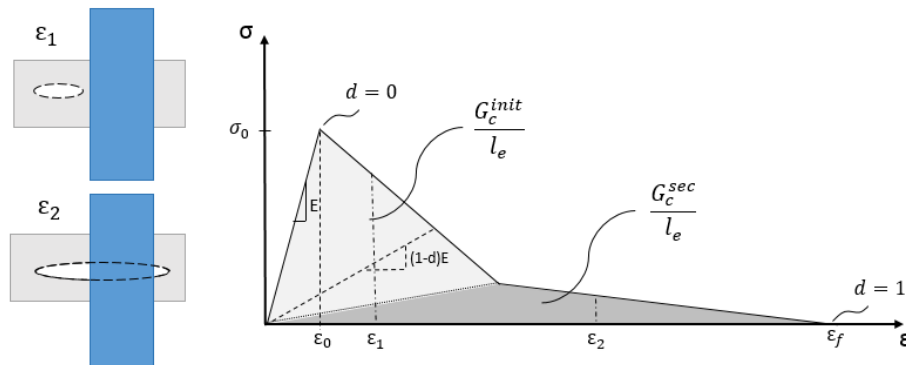


Figure 3.6: Bilinear damage law due to matrix entrapment.

The NCF model is very similar to that of the twill. The two differences are the lack of an unbreakable bond between 0 and 90 plies and no use of the bilinear damage model. No unbreakable bond is used since the stitching in the NCF used in this project is performed using a thermoplastic thread. The thread melts and loses its bounding effect during processing. Hence, the same contact condition as described in section 3.2.2 is used. There are however NCF materials with a stitching of glass fibre or other materials that are not affected by the heat during curing. For such NCF material an unbreakable bond should be considered. A linear damage model will be used since matrix entrapment will not occur in the same extent as for the twill when the layers are not weaved together.

3.4 Calibration of material parameters

The aim of this project was to produce a methodology that can be implemented with new layups and materials with ease. A detailed plan for the calibration of material parameters must therefore be included. This section details the calibration of a UD-ply and how to adapt these parameters to work for weaves and NCF.

3.4.1 UD-plies

The physical tests available on UD-plies at material level can be seen in *Figure 1.1*. Some of the material parameters were collected from these tests and others were estimated as seen below. A more detailed description of the procedure can be found in appendix B which contains a user guide on how to perform virtual material tests of CFRP.

Most of the material specific parameters could be extracted from available physical tests at material level, see *Table 3.1*. In addition to this, the out-of-plane shear strength (S_{13}) and an estimate of initial misalignment angle (ϕ_0) can be found from physical compression tests and the use of equations 3.1 and 2.8. According to the theory in section 2.1.3, α_0 is estimated to be 53° . All stiffnesses are taken as the initial slope of the stress-strain curve.

$$S_{13} = \frac{Y_c}{2 \cdot \tan(\alpha_0)} \quad (\text{Pinho et al., 2006a}) \quad (3.1)$$

A linear model was used for both in-plane and out-of-plane shear, see *Figure 3.7* and *3.8*. The in-plane shear strength (S_{12}) was taken where nonlinearity occurs in physical tests. The in-plane shear curve show small drops in stress at this point due to cracks in the test specimen. This together with the fact that the stiffness response becomes poor for higher strains are the reasons to why the in-plane shear strength is taken at this point.

The critical energy release rates in different modes can be measured in physical tests but were however not available for this project. The energy release rates are dependent on the micro-mechanical properties of fibres and matrix and how well these are bonded together (Beyerlein and Leigh Phoenix, 1997). This means that the energy release rates could be dependent on environmental conditions such as heat and moisture or the fibre architecture. The values from previously tested IM7/8552 were used for all architectures.

Two shear slope coefficients for Young's modulus, η_E , and shear modulus, η_G define the increase in stiffness due to friction appearing in cracks during compression loads. The values used for these parameters are shown in equation 3.2. These are the same values that were used for a number of similar materials during the second World Wide Failure Exercise (WWFE-II) according to Pinho, Darvizeh, Robinson, Schuecker, and Camanho (2012).

$$\eta_E = 16 \quad \eta_G = 0.2 \quad (3.2)$$

The strength slope coefficients found in equation 2.4 are estimated as in equation 3.3. These equations were proposed by Pinho et al. (2006a) during the development of the material model.

$$\eta_T = -\frac{1}{\tan 2\alpha_0} \quad \eta_L = -\frac{S_{12} \cos 2\alpha_0}{Y_c \cos^2 \alpha_0} \quad (3.3)$$

When all material parameters needed in the material model were collected, calibration towards the physical tests begun. The intention of the calibration strategy was to start with tests which are independent of material parameters calibrated later in the process. The order of calibration was as follows:

1. Make a virtual shear test on a $[0/90]_n$ UD-laminate at material level. Calibrate the in-plane shear strength, S_{12} , such that the failure stress in the virtual test correlate to the first indication of failure in the physical test.
2. Make a transverse virtual tensile test on a UD-laminate at material level. Calibrate the transverse tensile strength, Y_t and the transverse stiffness E_2 until the failure strength and strain is equal to the one of the physical test.
3. Make a longitudinal virtual tensile test on a UD-laminate at material level. Calibrate the longitudinal stiffness E_1 and the longitudinal tensile strength X_t until the failure stress and strain matches the ones of the physical tests.
4. Make a longitudinal virtual compression test on a UD-laminate at material level. Calibrate the initial fibre misalignment angle ϕ_0 such that the failure stress is equal in the virtual and physical tests.

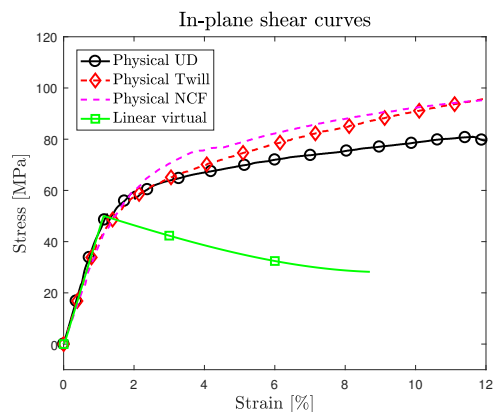


Figure 3.7: Curve fitment of in-plane shear.

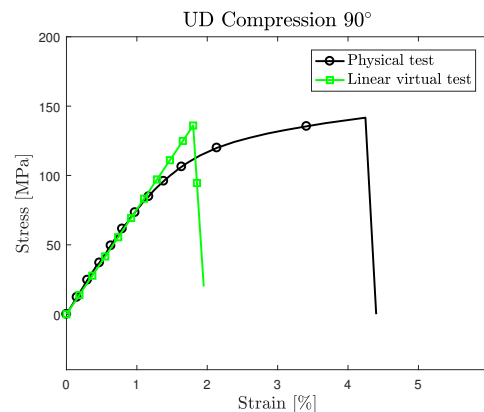


Figure 3.8: Curve fitment of transverse compression

3.4.2 Twill & NCF

It is expected that the longitudinal stiffness and strength, in both tension and compression have to be reduced due to fibre waviness in a twill or NCF. Physical tests of twill and NCF loaded in tension and compression along one of its fibre directions were available. During tensile loading, fibre tensile failure is the critical failure mode. Hence longitudinal stiffness and strength were used to calibrate a virtual model towards the physical test in tension. During compressive loading, fibre kinking is the driving failure mechanism. Hence the fibre misalignment angle was used to calibrate the virtual strength towards the physical tests in compression. The shear curves used were the same as the ones for UD-ply. This approximation is reasonable as seen in *Figure 3.7* and coincide with work by Medina, Canales, Arango, and Flores (2014) who states that the behaviour is similar. The methodology used to adjust the material properties from the calibrated UD-ply to be usable when modelling twill/NCF then reads as follows:

1. Calibrate the model in tension towards the physical tests of the twill/NCF. Use the longitudinal stiffness and strength to obtain a similar failure strength and strain as in the physical tests.
2. Calibrate the model in compression towards the physical tests of the twill/NCF. Use the fibre misalignment angle to calibrate the failure strength towards the physical tests.

3.4.3 Laminates

The laminates were tested using plies with the calibrated material parameters from previous section. In-situ strength was applied to UD-ply but not to twill and NCF. The reason to not use it for twill and NCF materials is that the material parameters are extracted and calibrated towards physical tests of twill and NCF, which are already laminated with fibres in different orientations.

3.5 Environmental effects on CFRP

Virtual material tests are also performed in two different environments. Those are Hot Temperature Wet (HTW, 80 °C) and Cold Temperature Dry (CTD, -40 °C) respectively. The methodology to collect and calibrate material data in these environments are somewhat changed compared to Room Temperature Dry (RTD). This will minimize the number of physical tests that have to be performed in HTW and CTD environments. Compared to room temperature, no physical tests in tension are done. Hence, Young's modulus for UD-ply in transverse and longitudinal directions (E_1 and E_2) are extracted from compression tests. The longitudinal tensile strength (X_t) is assumed to be the same as in room temperature since it is a fibre dominated property. The transverse tensile strength is calculated from 3.4.

$$Y_t = Y_t^{RTD} \frac{E_2}{E_2^{RTD}} \quad (3.4)$$

This was derived from equation 3.5 which is a way to find the transverse strength for linear stress-strain curves according to Agarwal, Broutman, and Chandrashekhara (2018). Gibson (2007) describes a method of how different matrix properties can be transformed between different temperatures by use of the same ratio, see equation 3.6. In these equations Y_{mt} is the matrix tensile strength, V_f is the fibre volume fraction and P represents an arbitrary matrix entity.

$$Y_t = Y_{mt} \frac{E_2}{E_m} (1 - V_f^{1/3}) \quad (3.5)$$

$$R_m = \frac{P_m}{P_{m0}} = \frac{E_m}{E_m^{RTD}} \quad (3.6)$$

Solving Y_{mt} from equation 3.5 in RTD environment and then multiplying with the ratio in equation 3.6 will give Y_{mt} in the new environment. Using this expression in equation 3.5 for the new environment and simplifying will result in equation 3.4.

The remaining UD-material parameters (Y_c , S_{13} , η_E , η_G , η_T , η_L and all critical energy release rates G_C) are collected using the same method as in section 3.4.1.

The calibration process also changes when testing in new environments. Both transverse and longitudinal stiffness are calibrated by compression tests instead of tension tests as earlier. Longitudinal tensile strength is not calibrated but this parameter should not change much anyway since it is a fibre dominated property. Hence the new calibration process reads as follows.

1. Make a virtual shear test on a $[0/90]_n$ UD-laminate at material level. Calibrate the in-plane shear strength, S_{12} , such that the failure stress in the virtual test correlate to the first indication of failure in the physical test.
2. Make a transverse virtual compression test on a UD-laminate at material level. Calibrate the transverse stiffness, E_2 , such that the virtual and physical tests have the same initial stiffness.
3. Make a longitudinal virtual compression test on a UD-laminate at material level. Calibrate the initial fibre misalignment angle ϕ_0 such that the failure stress is equal in the virtual and physical tests. Also calibrate the longitudinal stiffness, E_1 , such that the virtual and physical tests have the same initial stiffness.

To implement complex fabrics such as twill or NCF into new environments, it is first needed to do the above calibration on UD-ply. An assumption is then made that the ratio between a property of a UD-ply and of a fabric remain the same when changing environment. The new properties of a fabric can then be calculated e.g. as in equation 3.7. The parameters that need adjustment are longitudinal stiffness, E_1 , longitudinal tensile strength, X_t , and initial misalignment angle, ϕ_0 .

$$E_{1,Twill}^{HTW} = E_{1,UD}^{HTW} \frac{E_{1,Twill}^{RTD}}{E_{1,UD}^{RTD}} \quad (3.7)$$

4 Correlation and validation of test procedure

This chapter displays the correlations which validate the proposed methodology. It is important to have in mind that these results are not part of the expected outcome of this project. Their purpose is only to evaluate the procedure of chapter 5 and to show areas where improvements are necessary. Virtual tests were conducted to investigate how well the FE-model together with the material model can capture the material behaviour.

Correlation for the UD-model were found at an early stage of the project and worked as a guideline for further improvements of the methodology. Some changes to the UD-model were made after this stage in the project, which means that these numbers are not directly a result of the methodology described in chapter 3. However, UD-plyies are also involved in the laminates used to validate the twill/NCF model and the correlation at this stage is a direct representation of the methodology in chapter 3.

4.1 Correlation UD-model

Virtual tests on material IM7/8552 have been performed to validate the FE-model and the material model for UD-plyies. Correlation studies with known material parameters have previously been performed on this material. The virtual tests performed in this project are compared to physical tests on UD-laminates performed by Wisnom et al. (2010).

The layup used by Wisnom was $[45_m, 90_m, -45_m, 0_m]_{nS}$ where increasing m indicates ply scaling and increasing n indicates sublaminates scaling. For ply scaling n is kept equal to one and for sublaminates scaling m is kept equal to one. The ply thickness were 0.125 mm, hence the total laminate thickness, $t = n \cdot m$ (mm).

The ratio between specimen width and hole diameter was kept constant at five. Wisnom et al. (2010) used a gauge length of 20 times the hole diameter in open hole tests and 30 times the thickness in unnotched tests. Due to model size and calculation times these gauge lengths were not possible to replicate in the virtual tests. The gauge length was instead scaled to half of the length used in the physical tests. This only affected the strength of the specimen slightly since the gauge length is a dimension with low impact on the results. Moreover, since it was done consistently it was still possible to study trends in the behaviour which was the main purpose of these tests.

The intention with conducting tests on the IM7/8552-system were to highlight sensitive areas of the FE-model. Perfect correlation was not the objective at this stage. Thus, no calibration of material parameters was performed for tension tests. For compression, calibration on the initial misalignment angle (section 2.1.4) was done on the unnotched sublaminated scaled specimens.

Shown in *Table 4.1* and *4.2* are the results from the virtual and experimental tests for tension and compression, respectively. In most cases the compression tests show a better correlation to experiments than the tests in tension. The main reason for this is the calibration of the initial misalignment angle. Chen et al. (2012) have performed the same virtual tension tests using the same failure criteria as in this project. By comparison it is possible to see that the same material behaviour is captured. The results in this project have a larger error than the results presented by Chen et al. (2012). The reason for this is the lack of material parameter calibration at this stage of the project.

Table 4.1: Strength (MPa) of tension tests on IM7/8552. Physical tests by Wisnom et al. (2010) in parenthesis.

t (mm)	Sublaminated scaling (m=1,n=t)			
	Hole diameter (mm)			
	0	3.175	6.35	12.7
1	772 (842) -8.3 %	513 (570) -10 %		
2	835 (911) -8.3 %	521 (500) 4 %	457 (438) 4.3 %	
4	847 (929) -8.8 %	526 (478) 10 %	477 (433) 10.2 %	431 (374) 15.2 %
8		528 (476) 10.1 %		

t (mm)	Ply scaling (m=t,n=1)			
	Hole diameter (mm)			
	0	3.175	6.35	12.7
2	562 (660) -14.8 %	409 (396) 3.3 %	412 (498) -17.3 %	
4	380 (458) -17 %	295 (275) 7.3 %	315 (285) 10 %	280 (362) -22.7 %
8	287 (321) -10.6 %	226 (202) 11.9 %		

4. Correlation and validation of test procedure

Table 4.2: Strength (MPa) of compression tests on IM7/8552. Physical tests by Wisnom et al. (2010) in parenthesis.

t (mm)	Sublaminare scaling (m=1,n=t)		
	Hole diameter (mm)		
	0	6.35	12.7
2	629 (658) -4.4%	307 (338) -9.2%	
4	653 (675) -3.3%	344 (351) -2%	277 (301) -8%
8	648 (644) 0.6%		

t (mm)	Ply scaling (m=t,n=1)		
	Hole diameter (mm)		
	0	6.35	12.7
2	587 (666) -11.9%	400 (373*) 7.2%	
4	502 (642) -21.3%	395 (424) -6.8%	388 (348) 11.5%
8	483 (472) 2.3%		

Besides the correlation in strength prediction between virtual and physical tests, the trends of the material behaviour when scaling the test specimen in different ways are investigated. Considering the tensile tests, *Figure 4.1* shows the trends when scaling the thickness of an unnotched test specimen. Also looking at the scaling in hole diameter, the trends of a 4 mm thick test specimen is shown in *Figure 4.2*.

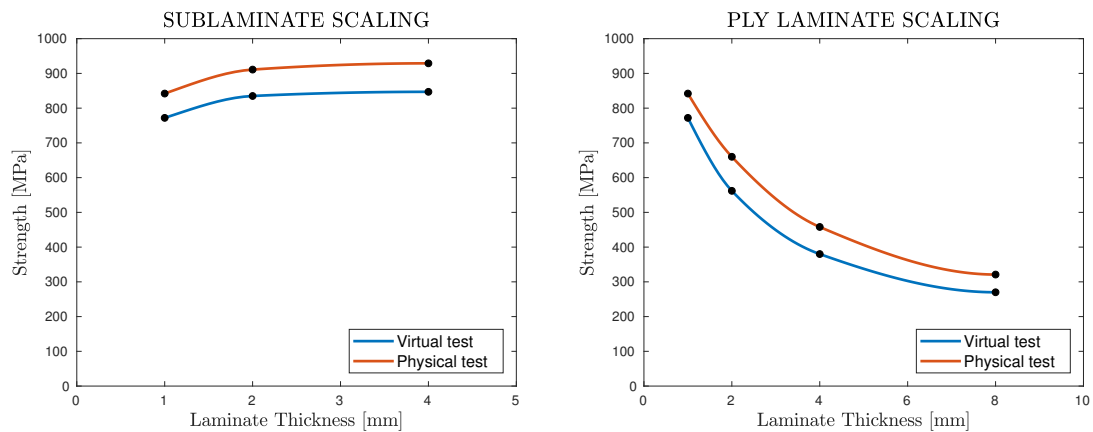


Figure 4.1: Trend in tensile strength of an unnotched specimen when scaling the laminate thickness for sublaminare scaling and ply laminate scaling respectively.

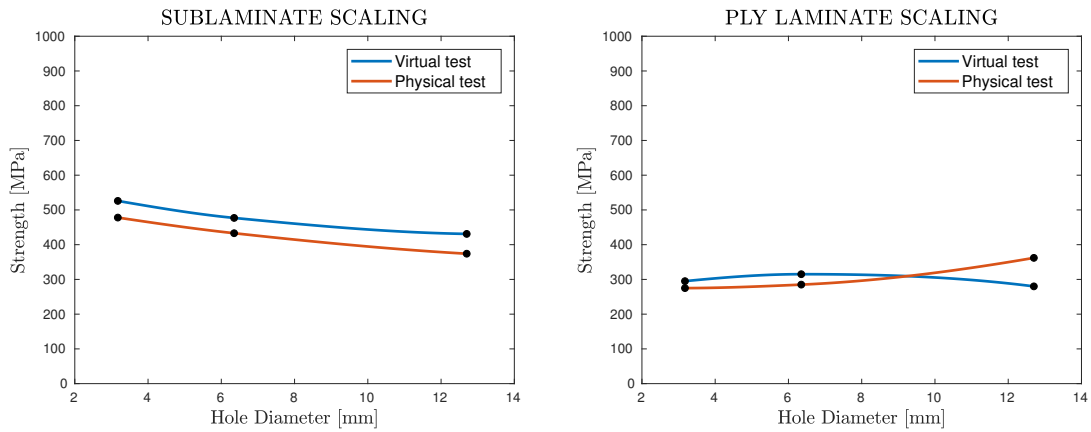


Figure 4.2: Trend in tensile strength of a notched specimen (laminate thickness 4 mm) when scaling the hole diameter for sublaminate scaling and ply laminate scaling respectively.

It can be concluded that the trends when scaling specimen size and hole diameter are mostly captured well during tensile loading. However, for ply scaled specimens it is possible to find a few tests that are not following the expected trends. These tests are consequently the largest scaled specimen tested at each laminate thickness.

In the same way as for tensile strength, the observed trends during compression is analysed. Since less tests were done in compression, some of the trends only have two points which makes it more difficult to draw any conclusions. Figure 4.3 shows the trends when scaling the laminate thickness for an unnotched test specimen. The trends for scaling of hole diameter with a thickness of 4 mm are shown in Figure 4.4.

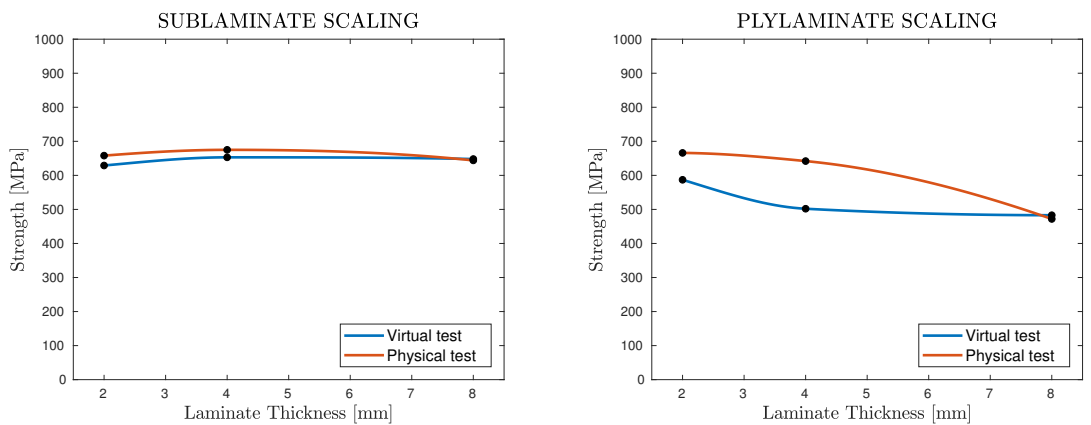


Figure 4.3: Trend in compressive strength of an unnotched specimen when scaling the laminate thickness for sublaminate scaling and ply laminate scaling respectively.

4. Correlation and validation of test procedure

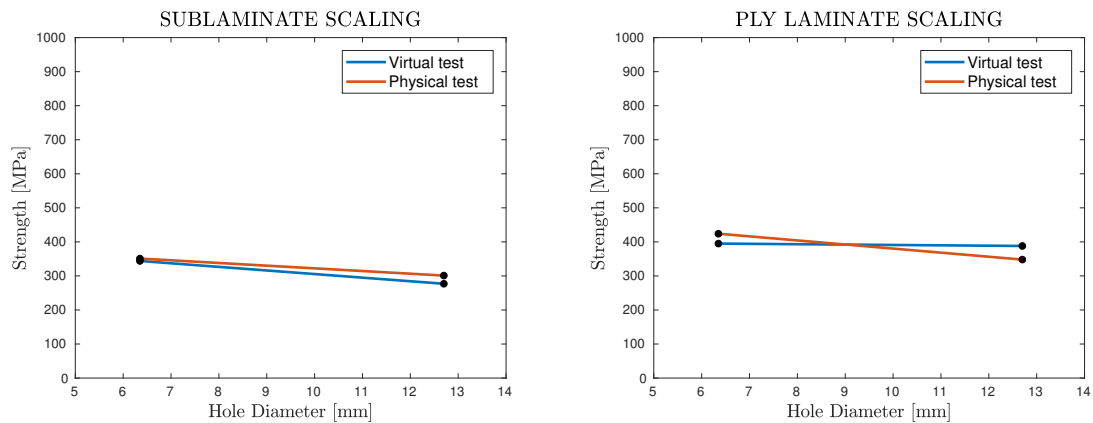


Figure 4.4: Trend in compressive strength of a notched specimen (laminate thickness 4 mm) when scaling the hole diameter for sublaminate scaling and ply laminate scaling respectively.

4.2 Correlation twill/NCF-model

Physical tests on laminates A, B and C, performed by Volvo Cars will be used to validate the virtual model including the proposed modelling technique for twill and NCF. This section gives a comparison between the virtual analysis performed with calibrated material parameters of T700/epoxy found in *Table A.1* and the physical data from experiments. The aim was to find a solution where failure stress and strain to failure coincide well with test data.

The results of the laminate simulations at RTD can be seen in *Figures 4.5-4.7*. The errors are in general below the targeted limit of 15%. The few that performed worse than the 15%-aim are open hole tests and unnotched compression tests.

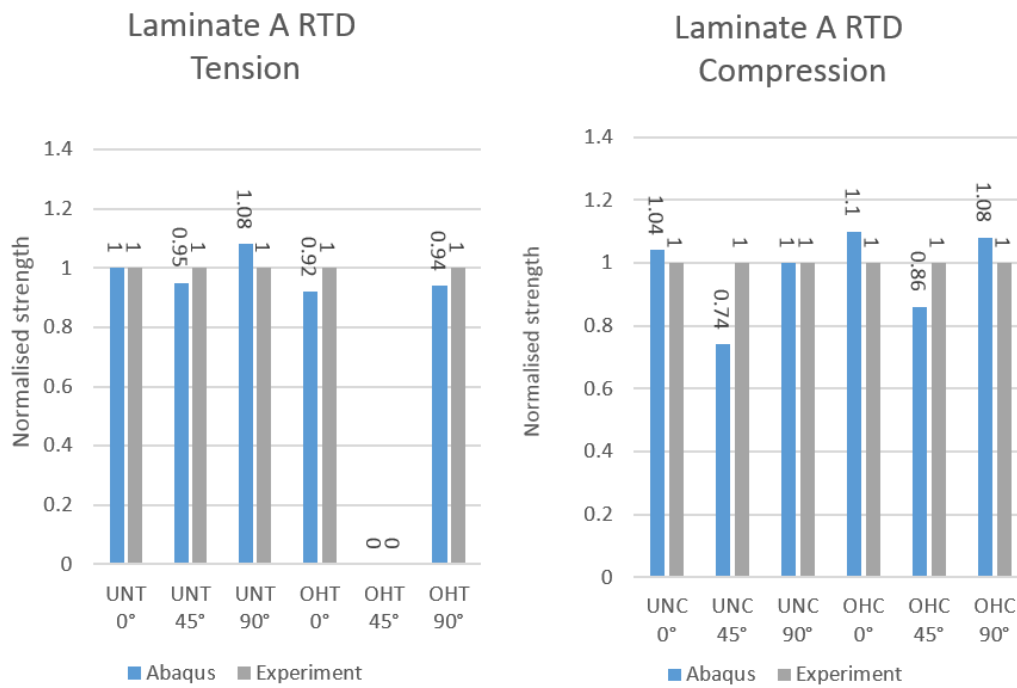


Figure 4.5: Results from simulation of laminate A in RTD compared to experiments.

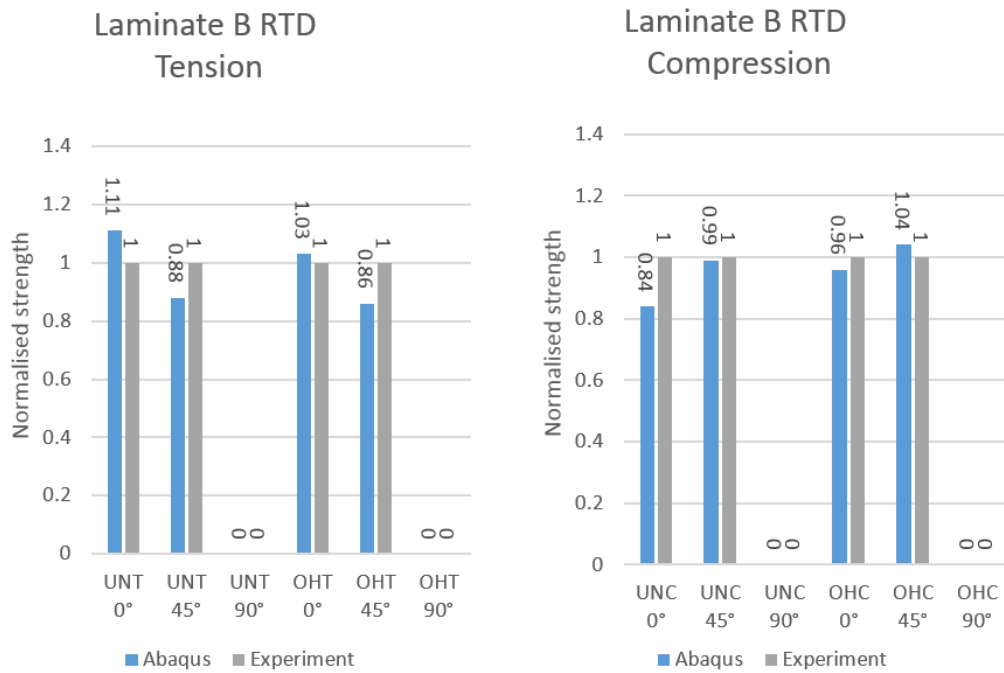


Figure 4.6: Results from simulation of laminate B in RTD compared to experiments.

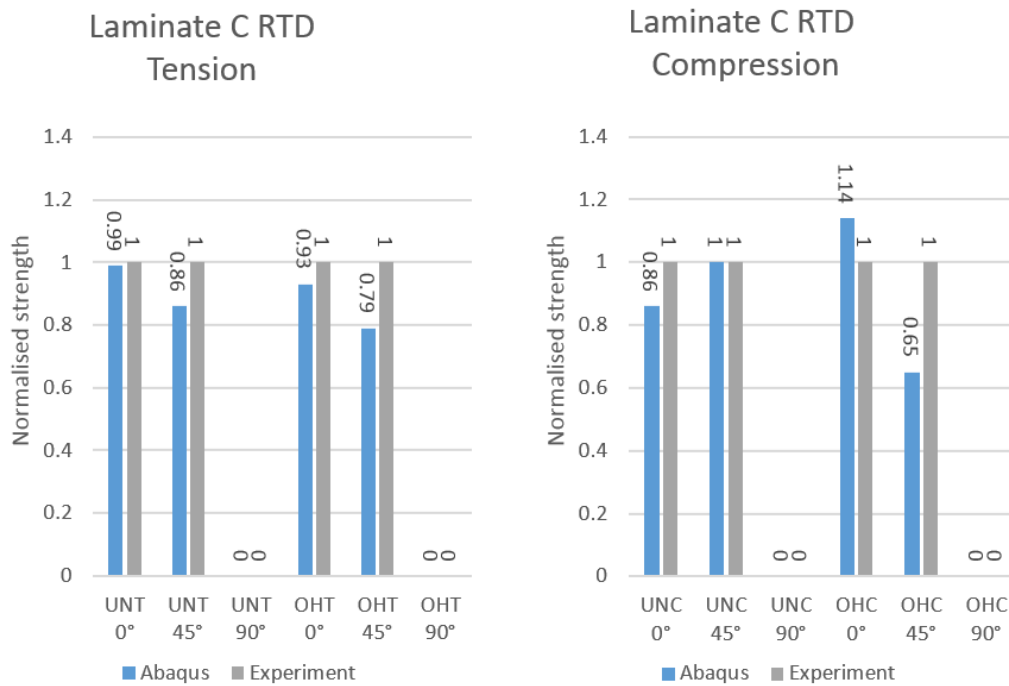


Figure 4.7: Results from simulation of laminate C in RTD compared to experiments.

The stress-strain response for some of the tests can be seen in *Figures 4.8-4.10*, stress-strain curves for all tests are found in Appendix C. The behaviour is well captured in most cases. There is a tendency to predict total failure where the first sign of failure occurs in the physical tests, seen in *Figure 4.9*. This behaviour comes mainly from the difference between a linear and a nonlinear shear response. The effects of which will delay the point of initial damage and will fail to capture the softening of the material.

Since these tests will be used as reference of strength when designing cars, no damage can therefore be allowed during normal use. A drop in stress can be seen at about 80% in *Figure 4.10*. A kink band is forming in an outer layer at this point which will therefore be considered the point of failure. The same approach has been applied to determine the reference strength from experimental tests, e.g the reference strength in *Figure 4.9* is set at about 80% of maximum value. The final strength is used as reference if the experimental tests has a smooth nonlinear behaviour as in *Figure 4.10*. No stress-strain curves were available for the physical tests on open hole specimens. The reference strength was therefore taken as the maximum strength for these tests.

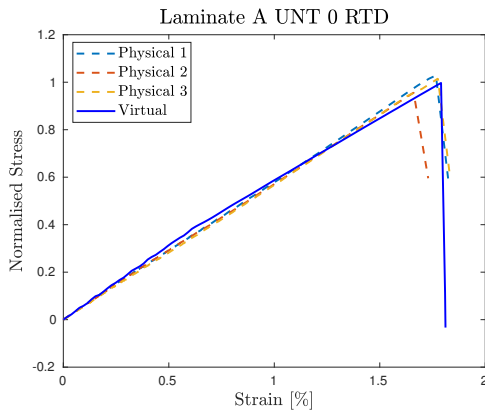


Figure 4.8: Stress-strain response of laminate A during unnotched tension in 0°

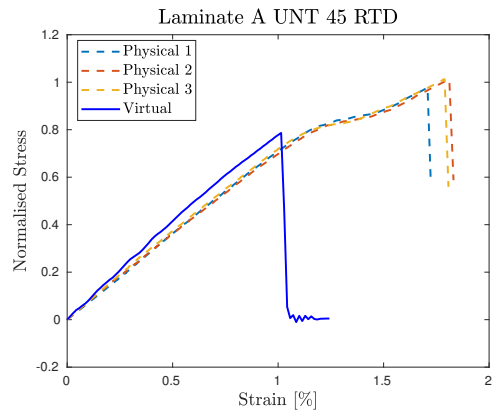


Figure 4.9: Stress-strain response of laminate A during unnotched tension in 45°

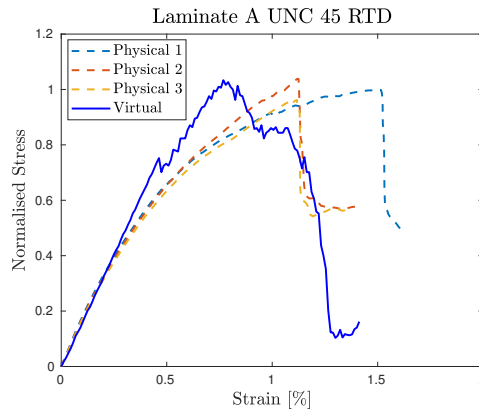


Figure 4.10: Stress-strain response of laminate A during unnotched compression in 45°

It is also possible to see that the same failure modes are simulated in the virtual tests as in the physical ones. *Figure 4.11* shows a delamination failure for a physical and a virtual test, respectively. In this case, the virtual test contains a symmetry plane which means that only half of the laminate is visible. This is the reason why only one delamination is visible in the virtual test. *Figures 4.12* and *4.13* show two more examples where a 45° matrix fracture and kink band are predicted.

4. Correlation and validation of test procedure

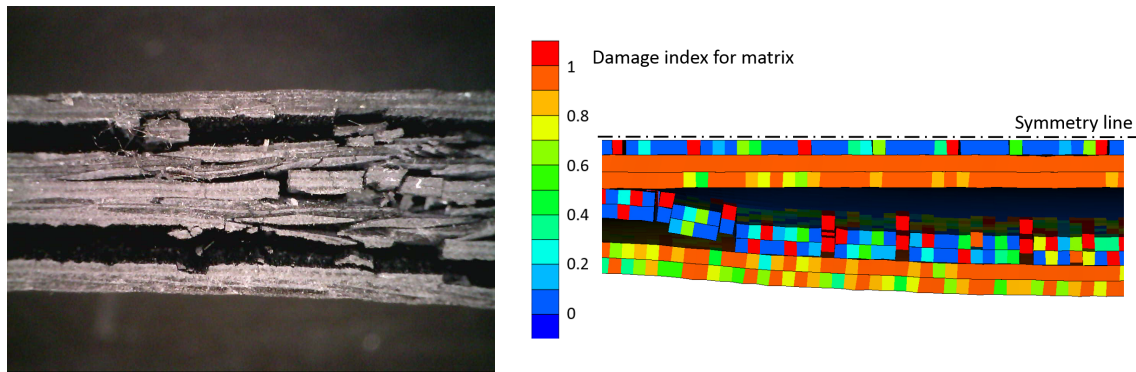


Figure 4.11: Delamination in a physical and a virtual test, laminate A, UNT 90°.

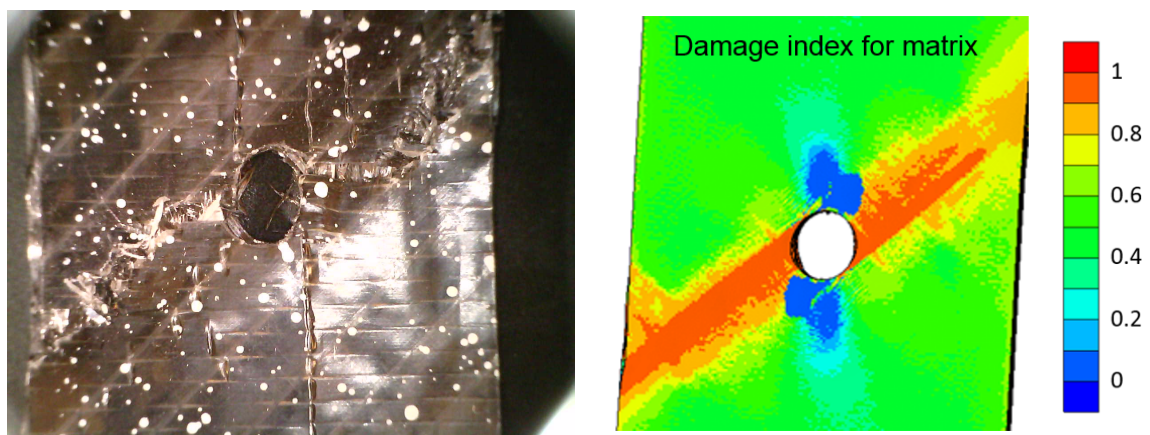


Figure 4.12: Matrix fracture in a physical and a virtual test, laminate B, OHT 45°.

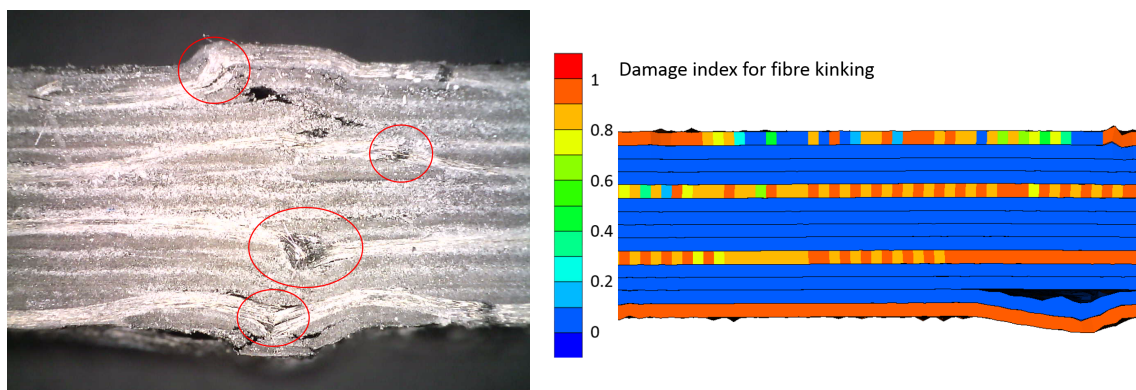


Figure 4.13: Fibre kinking in a physical and a virtual test, laminate A, UNC 45°.

4.3 Correlation environmental effects

The results for strength in other environments compared to experimental test are displayed in *Figures 4.14* to *4.17*. Significantly more assumptions had to be made while calibrating these parameters. This resulted in larger errors than at RTD. For CTD environments, the results are very similar to those in room temperature but the correlation for HTW environment is poor. The largest source of error seems to be the modelling of fibre kinking, this is discussed further in sections 6.4 and 6.5.

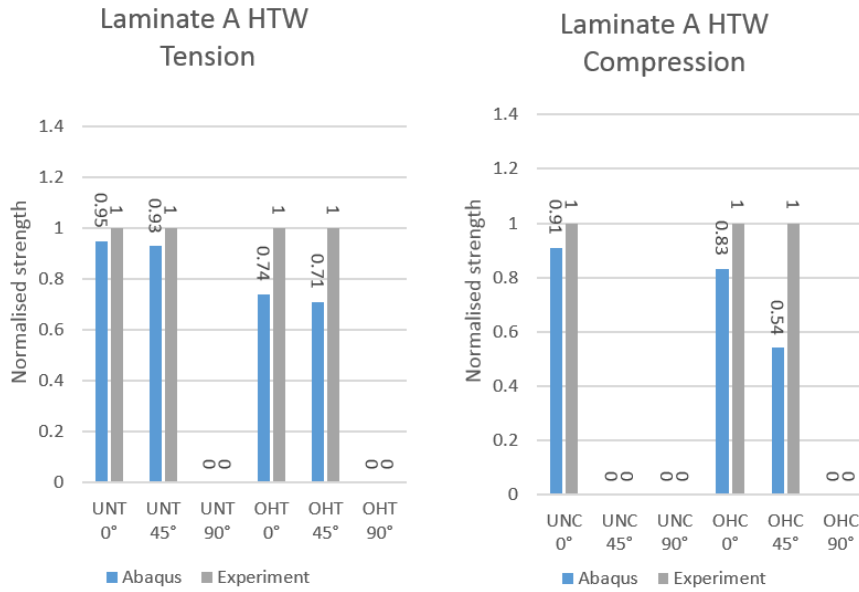


Figure 4.14: Results from simulation of laminate A in HTW compared to experiments.

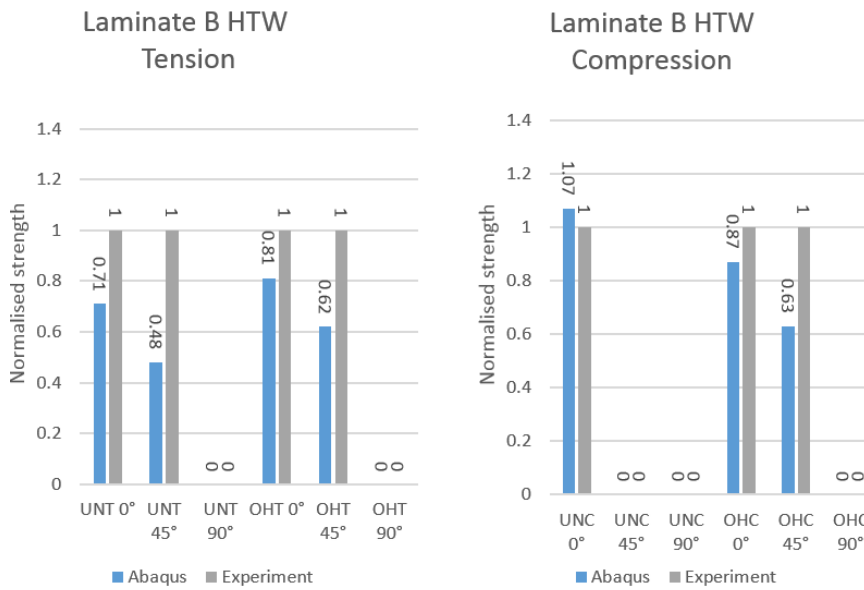


Figure 4.15: Results from simulation of laminate B in HTW compared to experiments.

4. Correlation and validation of test procedure

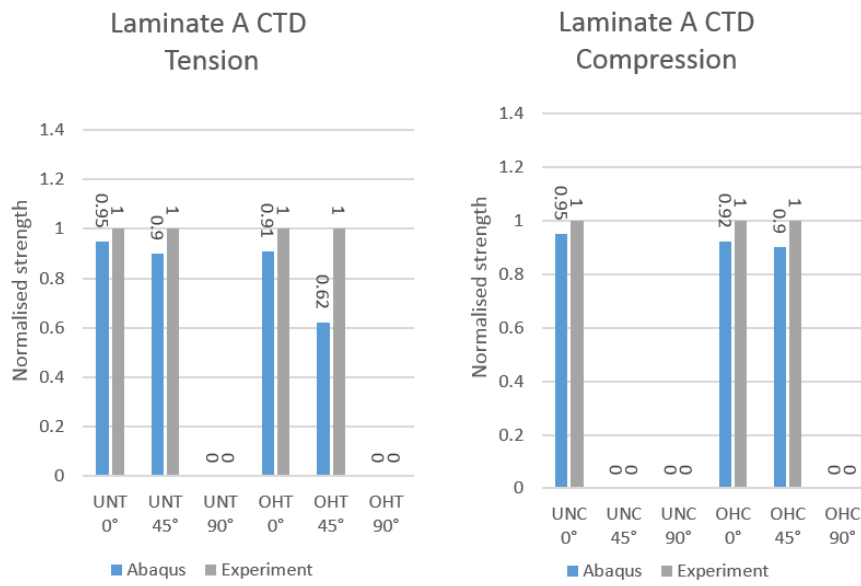


Figure 4.16: Results from simulation of laminate A in CTD compared to experiments.

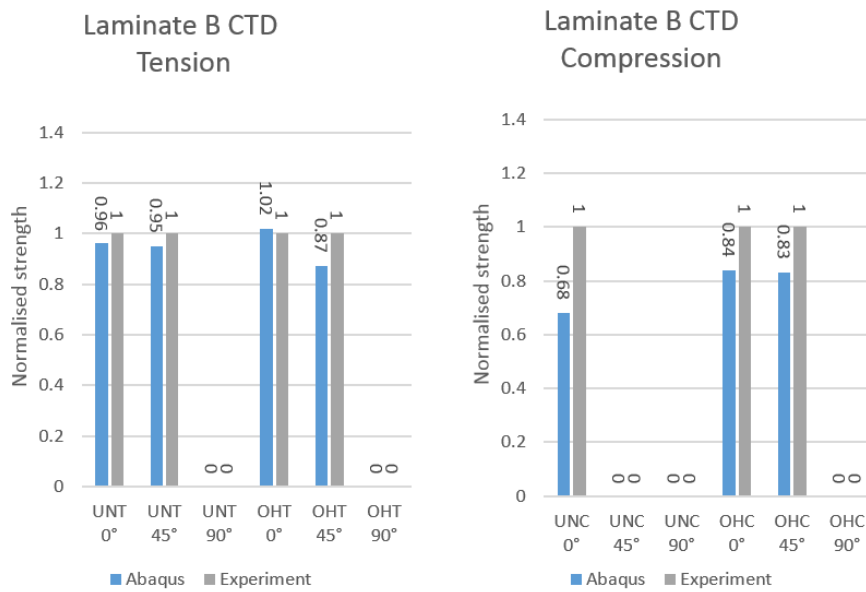


Figure 4.17: Results from simulation of laminate B in CTD compared to experiments.

5 Test procedure of new CFRP-materials

This section is dedicated to the procedure developed to conduct laminate tests on new materials. The FE-model used is the one described in section 3.2. Appendix B provides a detailed description on how to use the Python script, retrieve material parameters and calibrate towards physical tests.

The test procedure is visualized in *Figure 5.1*. Each arrow represent a flow of information necessary to continue the testing. The procedure is divided into two parts. The first step is to evaluate the material at RTD. This has to be the first step since many material properties at RTD are later transferred to other environments. When all material data has been collected at RTD for UD-plyes these can be transferred to other fibre architectures. This transfer is described in detail in section B.3.

When simulations are done at RTD, the other environments can be treated in a second step.

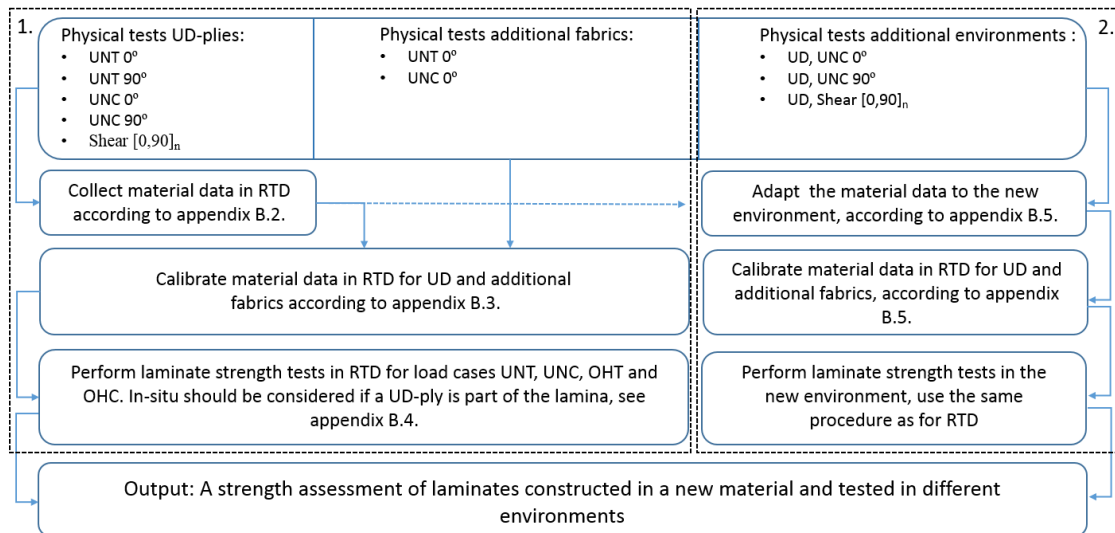


Figure 5.1: A flowchart of the suggested testing procedure to evaluate the strength of laminates in a new material.

6 Discussion

This chapter contains a discussion on the results from previous chapters and will look closer at the effects of possible error sources. Further, a discussion will be held on whether these error sources need to be accounted for in coming projects. The chapter will also cover most of the reasoning around choices that were made in order to move forward in the project.

6.1 Delamination

Green, Wisnom, and Hallett (2007) emphasize the large impact that the delamination process has on the failure stress. The effects of delamination should have its largest impact on ply scaled laminates with thick plies. During the validation of the UD-model it was possible to see this effect in *Figure 4.3*, where in ply scaling, delamination occurred in the 4mm thick virtual test. Wisnom et al. (2010) has not reported any delamination in the physical tests for this thickness, which might explain the difference in strength. The correlation was good when delamination occurred in both virtual and experimental tests for a thickness of 8mm. After this, a condition which disallowed delamination at the end tabs of the specimen were introduced. This gave improved delamination prediction in these laminates, seen in *Figure 6.1*.

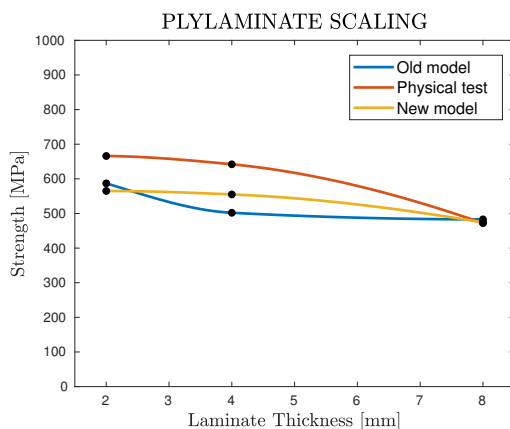


Figure 6.1: Trend in compressive strength of a unnotched specimen when scaling the thickness for ply laminate scaling.

Another factor that may cause inaccurate delamination predictions is the smeared crack model used in the virtual tests. This was proposed by Chen et al. (2012) who experienced a similar behaviour as was seen with large ply scaled specimens during validation of the UD-model in this project. The smeared crack model distributes cracks and stress concentrations over an element. Proper stress concentrations are thus lost, which will affect the crack propagation. There are several proposed remedies for this problem, for example to implement phantom nodes (van der Meer, Sluys, Hallett, and Wisnom, 2011) or to use an adaptive fidelity shell model (McElroy et al., 2017). However, the results can be considered good enough not to implement any of these methods.

6.2 In-situ strength

Another factor that may affect the results is the use of in-situ strength where non-linear shear curves has to be extrapolated. Depending on how this extrapolation is done, the transverse tensile and shear strengths on ply level will differ. This might explain why some of the values show poor correlation to values from the physical tests.

The use of in-situ strength were also evaluated while modelling fabrics. The NCF has thin layers and may therefore benefit from in-situ strength. It has been tested to simulate some laminates with in-situ strength on the NCF. However, it was concluded that the consideration of in-situ strength resulted in worse correlation to physical tests. A possible reason for this is that the in-situ strength has already been captured during the calibration process. Another plausible explanation is that the mechanisms that give rise to in-situ could have a smaller impact on more complex structures.

6.3 Stiffness

It can be concluded from the physical tests that tensile and compressive stiffness differs slightly. The stiffness of the NCF at RTD tension was on average 58 MPa and in compression 65 MPa. The FE-model was able to capture this rather well with a stiffness of 58.6 MPa in tension and 62.8 MPa in compression. Since the material model with the current settings only allows for one stiffness input it was calibrated against the stiffness in tension which is less affected by other material mechanisms. A similar but less severe behaviour was observed for both twill and UD-plyies.

The difference in stiffness increased in the HTW environment such that the material model was unable to capture it well. This was not accounted for in order to keep the simplicity of the methodology. One explanation for the increased difference in stiffness is that a temperature of 80 °C for a soaked specimen will be close to the glass transition temperature of the matrix. Accordingly there is significant change in material response to expect in such an environment (Wang et al., 2011).

Naya, Herráez, Lopes, Gonzáles, van der Veen, and Pons (2017) discuss the stiffness decrease following an increase in fibre misalignment angle. However, this phenomenon tends to behave differently in a HTW environment compared to RTD environment. There were no possibility to include this consideration in the methodology due to lack of applicable research. The assumption made in this project was that the same reduction factor is used for transforming properties from UD to twill or NCF, independent of the environment. This could cause the overprediction in stiffness found in most HTW test, e.g. seen in *Figure 6.2.a*. A remedy for this would be to preform physical compression tests on twill and NCF in HTW which is suggested for future projects. This would allow for calibration of stiffness and initial misalignment angle.

6.4 Kink band prediction

Compressive material tests were available for twill and NCF at RTD, therefore calibration of initial misalignment angle was possible. This resulted in predictions of strengths that were close to experimental results. However, assumptions about the initial misalignment angle had to be made for CTD and HTW due to the lack of experimental data. These assumptions proved to be inaccurate leading to poor correlation with compression test results where a twill or NCF were oriented 0° to the load.

6.5 Transverse fibre kinking

An interesting behaviour occurred in some of the tensile tests at RTD and HTW. It can be observed that the virtual model predicted fiber kinking in plies oriented 90° to the load, described in *Figure 6.2*. With the current settings, only one failure mode can be activated for an element in the applied material model. The result of this becomes a slower damage propagation since the fibre kinking mode has a higher energy release rate than matrix failure. This in itself has a small impact on the overall strength of these tests and could be solved by allowing more than one failure mode in each element. However, the predictions are not very accurate. Looking at the test coupons from experiments shows no sign of fibre kinking in tension tests at RTD. Since the damage in some cases propagates into neighbouring plies, this will result in too early failure.

In the same way as for room temperature tests, the tension tests in new environments for laminates B and C show significant fibre kinking failure in 90° plies. The softer matrix in HTW environment results in a much larger matrix damage in neighbouring plies due to the fibre kinking. This explains the inaccurate results for tension tests in HTW environments. A solution that was tested was to set the fibre misalignment angle equal zero in all tension tests. This solved the problem in most cases, seen in *Figure 6.3.b*. However, in some cases it can be seen from the physical test coupons that a possible transverse fibre kinking failure actually happened in surface plies, see *Figure 6.4*. In these cases the strength would be heavily overpredicted if the misalignment angle was changed to zero. This can be seen in *Figure 6.3.a*. There was no effect of changing ϕ_0 for coupons that did not trigger the kinking mode, seen in *Figure 6.3.c*.

A more physically based approach to address the transverse kinking behaviour was to question that no delamination could form in the twill. Large delamination in a twill ply are not possible. However, it can happen that micro delaminations form, reducing the ability to transfer shear forces from one fibre bundle to another. The trilinear law of matrix damage in *Figure 3.6* was replicated with the use of an exponential damage law for contacts in a twill. It can be seen in *Figure 6.3.a* that the kinking behaviour can be controlled via this method. But the method is very parameter sensitive, dependent on strengths, stiffnesses and energy release rates of the contact. A combination of parameter values that resulted in the correct failure mode for all tests was not found. This method can be promising if accurate parameter values are available from experiments. This project did not have the time to investigate how one could predict this failure any further. Hence it is left for future work.

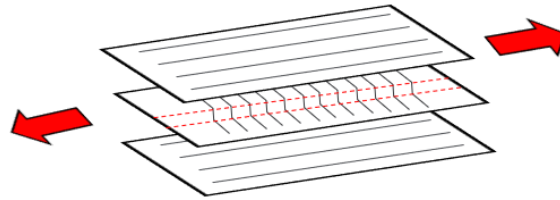


Figure 6.2: Fibre kinking in a ply where fibres are oriented 90° to the load.

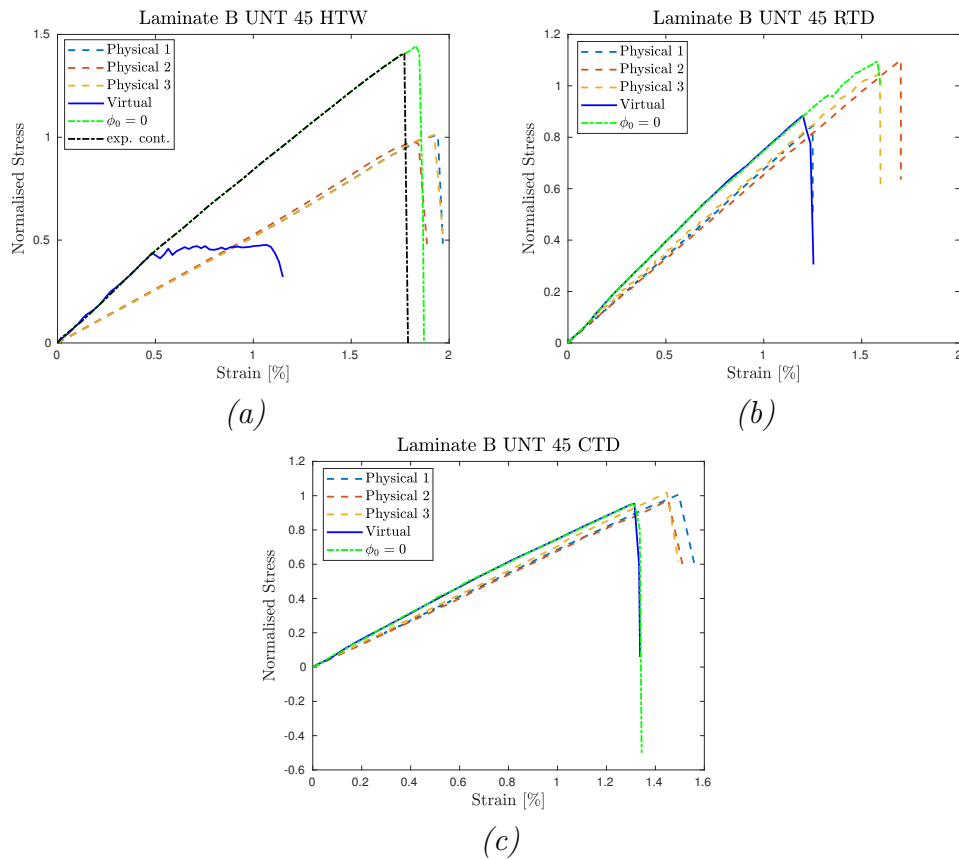


Figure 6.3: Influence of $\phi_0 = 0$ for different environments.

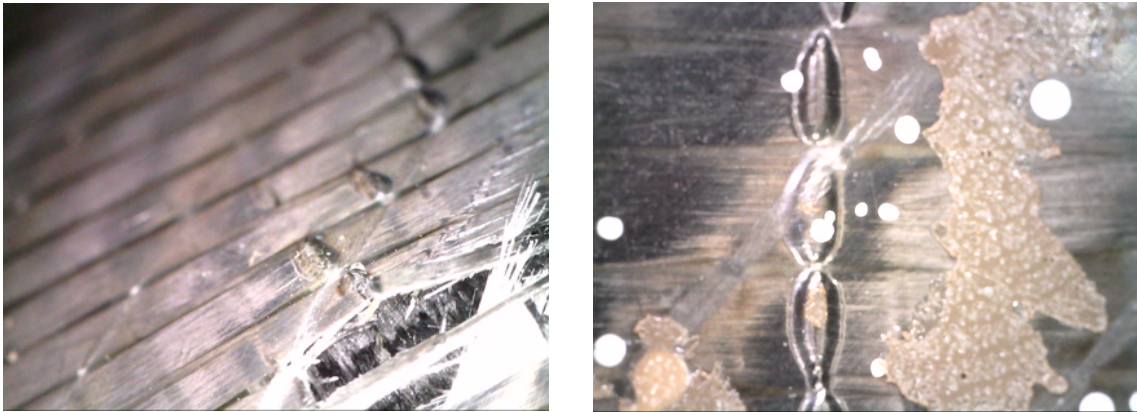


Figure 6.4: Possible fibre kinking in a transverse NCF ply at the surface.

6.6 Nonlinear shear

The physical tests showed a nonlinear shear behaviour, both in- and out-of-plane. A nonlinear shear response in the virtual tests was thus evaluated as well. A polynomial representation of the stress-strain response was implemented in the FE-code. On material level this resulted in a better stress-strain response, see *Figures 6.5* and *6.6*. This method was however complex to implement and difficult to combine with the use of in-situ strength. When tested on laminate level it turned out to be unstable and the linear model provided more accurate results. However, since it proved to work well on material level it is recommended to look deeper into this modelling technique in future work.

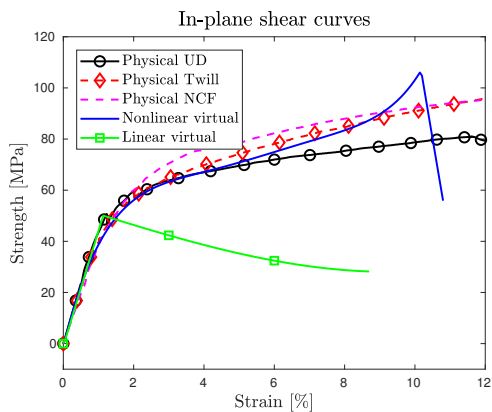


Figure 6.5: Curve fit of in-plane shear.

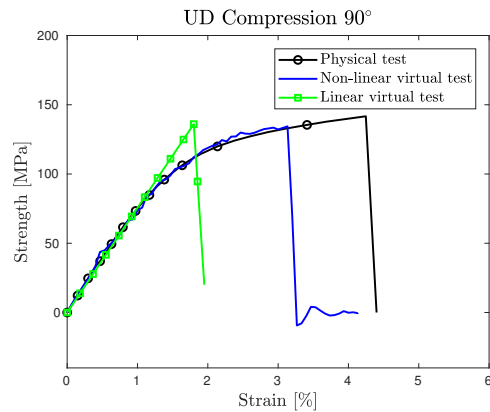


Figure 6.6: Curve fit of transverse compression

6.7 Environmental effects on CFRP

An assumption when testing the materials in new environments was that the properties of the fibres would remain unaffected. This assumption is questionable, resulting in a too stiff response compared to the physical tests. This led to a reduction of the longitudinal stiffness, E_1 . This also applies to the compressive strength, leading to a recalibration of the initial misalignment angle when testing new environments. It was hard to find any research about the mechanism that causes a change in fibre behaviour. The best explanation found was that heat and moisture affects the bonding between matrix and fibres as mentioned in section 2.4 (Wang et al., 2011).

6.8 Additional error sources

Most cases with errors larger than 15% compared to physical tests were open hole tests in both tension and compression on laminate C loaded in 45° loading angle. The stress state around a hole is hard to predict in a non-isotropic material such as CFRP. Further, stress-strain curves were not available for these tests and made it impossible to see the first sign of failure. Hence, comparisons were made towards final strength. These factors combined, resulted in less accurate predictions for these tests.

7 Conclusions and Future work

A methodology has been suggested for virtual material testing of laminates based on physical tests at material level, found in appendix B. For room temperature, the correlation with physical tests can be deemed satisfactory when it comes to predicting first sign of failure. This means that physical tests on laminate level, in tension and compression at RTD environment, can be substituted with virtual tests. Further, no shear tests on fabrics like twill or NCF are needed.

A method for transforming material properties from room conditions (RTD) into other environments has also been developed. However, the results in HTW environment shows a significant difference compared to physical tests. The developed methodology is not accurate enough in predicting kink bands for environments like this. A difference in stiffness between physical and virtual tests is also present at some tests in the HTW environment. Hence, it is recommended to perform physical compression tests on twill and NCF so that the kink angle and stiffness can be calibrated in the same way as suggested for room temperature. The prediction of fibre kinking and stiffness for twill and NCF in HTW environments have to be further investigated in future work.

The methodology gives better correlation in CTD environment and most tests are accurate. However, it can be concluded that one compression test has an unsatisfying difference in strength. It is thus necessary to investigate the prediction of kink bands for the CTD environment as well. *Figure 7.1* shows which tests are needed and which tests that can be simulated with confidence, using the developed methodology.

The model needs to be developed and evaluated for more load scenarios, such as shear and out-of-plane bending. This in order to fully substitute experimental tests. This was outside the scope of this project but is left as a possible continuation.

		T700-DT120				LAMINATES TESTED							
RTD - Room Temperature	LOAD	Twill		UD	NCF	LAMINATE A			LAMINATE B		LAMINATE C		
		0°	0°	90°	0°	0°	45°	90°	0°	45°	0°	45°	
RTD - Room Temperature	TENSION	X	X	X	X	+	+	+	+	+	+	+	UNT
						+	+	+	+	+	+	+	OHT
	COMPRESSION	X	X	X	X	+	+	+	+	+	+	+	UNC
						+	+	+	+	+	+	+	OHC
	SHEAR		X										
HTW - Hot / Wet +80	LOAD	Twill		UD	NCF	LAMINATE A			LAMINATE B		LAMINATE C		
		0°	0°	90°	0°	0°	45°	90°	0°	45°	0°	45°	
HTW - Hot / Wet +80	TENSION					?	?	?	?	?	?	?	UNT
						?	?	?	?	?	?	?	OHT
	COMPRESSION	!	X	X	!	?	?	?	?	?	?	?	UNC
						?	?	?	?	?	?	?	OHC
	SHEAR		X										
CTD - Cold / Dry -40	LOAD	Twill		UD	NCF	LAMINATE A			LAMINATE B		LAMINATE C		
		0°	0°	90°	0°	0°	45°	90°	0°	45°	0°	45°	
CTD - Cold / Dry -40	TENSION					+	+	+	+	+	+	+	UNT
						+	+	+	+	+	+	+	OHT
	COMPRESSION	!	X	X	!	?	?	?	?	?	?	?	UNC
						?	?	?	?	?	?	?	OHC
	SHEAR		X										

Figure 7.1: Cross - Necessary tests to perform the methodology. Plus sign - Tests that are simulated with the developed methodology. Exclamation mark - Tests that are recommended to develop the methodology further. Question mark - Tests that may be possible to simulate if the recommended tests are available.

References

- B.D. Agarwal, L.J Broutman, and K. Chandrashekhara. Analysis and performance of fiber composites, 2018. Hoboken: John Wiley & sons. Inc.
- AS Argon. Fracture of composites, 1972. *Treatise on Materials Science and Technology*. New York: Academic press 1, 79-114.
- ASTM. ASTM D5379 / D5379M-12, standard test method for shear properties of composite materials by the v-notched beam method, 2012. ASTM International, West Conshohocken, PA, 2012, Collected 2019-05-09 at <https://www.astm.org/>.
- ASTM. ASTM D6641 / D6641M-16e1, standard test method for compressive properties of polymer matrix composite materials using a combined loading compression (clc) test fixture, 2016. ASTM International, West Conshohocken, PA, 2016, Collected 2019-05-09 at <https://www.astm.org/>.
- ASTM. ASTM D3039 / D3039M-17, standard test method for tensile properties of polymer matrix composite materials, 2017. ASTM International, West Conshohocken, PA, 2017, Collected 2019-05-09 at <https://www.astm.org/>.
- I.J. Beyerlein and S. Leigh Phoenix. Stress profiles and energy release rates around fibre breaks in a lamina with propagating zones of matrix yielding and debonding, 1997. *Composites Science and Technology*, 51, 869-885.
- P.P Camanho, C.G. Dávila, S.T. Pinho, L. Iannucci, and P. Robinson. Prediction of in situ strengths and matrix cracking in composites under transverse tension and in-plane shear, 2006. *Composites Part A: Applied Science and Manufacturing*, 37, 165-176.
- B.Y. Chen, T.E. Tay, P.m. Biaz, and S.T. Pinho. Numerical analysis of size effects on open-hole tensile composite laminates, 2012. *Composites Part A: Applied Science and Manufacturing*, 47, 52-62.
- G. Gardiner. *Accelerating materials insertion: Where do virtual allowables fit?*, 2017. Collected 2019-01-25 at <https://www.compositesworld.com/articles/accelerating-materials-insertion-where-do-virtual-allowables-fit>.
- R.F. Gibson. Principles of composite material mechanics: Second edition, 2007. Boca Raton: Taylor Francis Group.
- B.G. Green, M.R. Wisnom, and S.R. Hallett. An experimental investigation into the tensile strength scaling of notched composites, 2007. *Composites Part A: Applied Science and Manufacturing*, 38, 867-878.
- E.S. Greenhalgh. Failure analysis and fractography of polymer composites: A volume in woodhead publishing series in composites science and engineering, 2009. Boca Raton: Woodhead Publishing Limited.
- R. Gutkin, M.L. Laffan, S.T. Pinho, P. Robinson, and P.T. Curtis. Modelling the

- r-curve effect and its specimen-dependence, 2011. *International Journal of Solids and Structures*, 48, 1767-1777.
- A.S Kaddour and M.J Hinton. Challenging lessons from the second world wide failure exercise (WWFE-II): Predicting failure in polymer composite laminates under 3-d states of stress, 2013. *International conference on composite materials*, 19.
- M.W. McElroy, R. Gutkin, and M. Pankow. Interaction of delaminations and matrix cracks in a cfrp plate, part II: Simulation using an enriched shell finite element model, 2017. *Composites Part A: Applied Science and Manufacturing*, 103, 252-262.
- C. Medina, C. Canales, C. Arango, and P. Flores. The influence of carbon fabric weave on the in-plane shear mechanical performance of epoxy fiber-reinforced laminates, 2014. *Journal of Composite Materials*, 48, 2871.
- F. Naya, M. Herráez, C.S. Lopes, C. Gonzáles, S. van der Veen, and F. Pons. Computational micromechanics of fiber kinking in unidirectional frp under different environmental conditions, 2017. *Composites Science and Technology*, 144, 26-35.
- S.T. Pinho, L. Iannucci, and P. Robinson. Physically-based failure models and criteria for laminated fibre-reinforced composites with emphasis on fibre kinking: Part I: Development, 2006a. *Composites Part A: Applied Science and Manufacturing*, 37, 63-73.
- S.T. Pinho, L. Iannucci, and P. Robinson. Physically-based failure models and criteria for laminated fibre-reinforced composites with emphasis on fibre kinking: Part II: Fe implementation, 2006b. *Composites Part A: Applied Science and Manufacturing*, 37, 766-777.
- S.T. Pinho, R. Darvizeh, P. Robinson, C. Schuecker, and P.P. Camanho. Material and structural response of polymer-matrix fibre-reinforced composites, 2012. *Journal of Composite Materials*, 46, 2313-2341.
- F.P. van der Meer, L.J. Sluys, S.R. Hallett, and S.R. Wisnom. Computational modeling of complex failure mechanisms in laminates, 2011. *Journal of Composite Materials*, 46(5), 603-623.
- K. Wang, B. Young, and S.T. Smith. Mechanical properties of pultruded carbon fibre-reinforced polymer (cfrp) plates at elevated temperatures, 2011. *Engineering Structures*, 33, 2154-2161.
- M.R. Wisnom, S.R. Hallett, and C. Soutis. Scaling effects in notched composites, 2010. *Journal of composite materials*, vol.44, No.2/2010.

Appendices

A Calibrated material data

Table A.1: Calibrated material parameters used in this project (in-situ strength is not included here).

Material properties						
Property		Unit	IM7/8552	T700/epoxy	T700 Twill*	T700 NCF*
Longitudinal modulus	E_1	GPa	171.42	130	130	120
Transverse modulus	E_2	GPa	9.08	7.5	7.5	7.5
Major Poisson's ratio	ν_{12}		0.32	0.3	0.3	0.3
Major transverse Poisson's ratio	ν_{23}		0.5	0.4	0.4	0.4
In-plane shear modulus	G_{12}	GPa	5.29	4.5	4.5	4.5
Longitudinal tensile strength	X_T	MPa	2326	2365	1920	1960
Longitudinal compressive strength	X_C	MPa	1590	900	725	730
Transverse tensile strength	Y_T	MPa	62.3	40	40	40
Transverse compressive strength	Y_C	MPa	199.8	140	140	140
In-plane shear strength	S_{12}	MPa	92.3	80	80	80
Fracture angle pure transverse	α_0	°	53	53	53	53
Initial kinking angle	ϕ_0	°	2	4.5	5.5	5
Transverse shear strength	S_{13}	MPa	75.28	80	80	80
Longitudinal shear strength slope coeff.	η_L		0.35	0.43	0.4	0.43
Transverse shear strength slope coeff.	η_T		0.29	0.29	0.29	0.29
Transverse Young's modulus slope coeff.	η_E		16	16	16	16
Shear modulus slope coeff.	η_G		0.2	0.2	0.2	0.2
Critical energy release rate fibre tension	$G_C^{FT,mit}$	kJ/m ²	97.8	97.8	97.8	97.8
Critical second energy release rate fibre tension	$G_C^{FT,sec}$	kJ/m ²	35.5	35.5	35.5	35.5
Ratio strength over 2nd failure process strength	r^{FT}		0.0084	0.0084	0.0084	0.0084
Critical energy release rate kinking	$G_C^{KINK,mit}$	kJ/m ²	106.3	106.3	106.3	106.3
Critical second energy release rate kinking	$G_C^{KINK,sec}$	kJ/m ²				
Ratio strength over 2nd failure process strength	r^{KINK}					
Critical energy release rate matrix mode I	$G_C^{MI,mit}$	kJ/m ²	0.2774	0.256	0.256	0.256
Critical second energy release rate matrix mode I	$G_C^{MI,sec}$	kJ/m ²			1.626	
Ratio strength over 2nd failure process strength	r^{MI}				0.0108	
Critical energy release rate matrix mode II	$G_C^{MII,mit}$	kJ/m ²	0.7874	0.7874	0.7874	0.7874
Critical second energy release rate matrix mode II	$G_C^{MII,sec}$	kJ/m ²			5.0012	
Ratio strength over 2nd failure process strength	r^{MII}				0.01	
Critical energy release rate matrix mode III	$G_C^{MIII,mit}$	kJ/m ²	0.7874	0.7874	0.7874	0.7874
Critical second energy release rate matrix mode III	$G_C^{MIII,sec}$	kJ/m ²			5.0012	
Ratio strength over 2nd failure process strength	r^{MIII}				0.01	

* Material properties of UD-ply used to build the fabrics

Table A.2: Properties that are changed when solving for a strictly linear model (in-situ strength is not included here).

Material properties (linear)						
Property		Unit	IM7/8552	T700/epoxy	T700 Twill*	T700 NCF*
Longitudinal modulus	E_1	GPa	-	132	-	-
Longitudinal tensile strength	X_T	MPa	-	2390	-	-
In-plane shear strength	S_{12}	MPa	-	50	50	50
Initial kinking angle	ϕ_0	°	-	2.7	3.25	3.1
Transverse shear strength	S_{13}	MPa	-	52.75	52.75	52.75
Longitudinal shear strength slope coeff.	η_L		-	0.27	0.27	0.27
Transverse shear strength slope coeff.	η_T		-	0.29	0.29	0.29

* Material properties of UD-ply used to build the fabrics

B User guide for virtual material testing

This is a detailed step by step guide that explains how to perform virtual material tests on laminate level for a carbon fibre composite. Before starting, the following physical material tests have to be available:

- UNT tests in 0° of UD-laminate on material level for all involved materials.
- UNT tests in 90° of UD-laminate on material level for all involved materials.
- UNC tests in 0° of UD-laminate on material level for all involved materials
- UNC tests in 90° of UD-laminate on material level for all involved materials.
- Shear tests of UD-laminate $[0/90]_n$ on material level for all involved materials.

If a non-UD fabric like NCF or weave is involved in any of the layups. Then the following following physical tests have to be performed on these fabrics for all involved materials:

- UNT tests in 0° of a Weave/NCF-laminate on material level.
- UNC tests in 0° of a Weave/NCF-laminate on material level.

Further, if tests are to be performed in several environments then the following physical tests are needed in these environments:

- UNC tests in 0° of UD-laminate on material level for all involved materials.
- UNC tests in 90° of UD-laminate on material level for all involved materials.
- Shear tests of UD-laminate $[0/90]_n$ on material level for all involved materials.

B.1 Building the FE-model

The FE-model is provided via *ANSA* and the python script `Build_CFRP_coupon.py`. This section will step by step go through how to use this script. The units for this script will be MPa for all stresses and stiffnesses, mm for dimensions, s for time and $^\circ$ for angles.

1. Open the script in the *ANSA* script editor. The settings needed to produce an *Abaqus* input file will be found at the top of the script see *Figure B.1*.

```

27 # Settings main
28 L =12.7 # [mm] length of coupon
29 W =13 # [mm] width of coupon
30 D =0 # [mm] hole diameter, 0=unnotched
31 el_length = 0.25 # [mm] length of elements on perimeter
32 LOAD_CASE = 'Compression' # set loadcase ("Compression" or "Tension","Shear")
33 STOP_time = 0.018 # End of intervall
34 Step_length = 0.00018 # set intervall step length
35 Laminate_rotation=45 # rotate the whole lamina said degrees anti clockwise

```

Figure B.1: Main settings for script.

- The coupon dimensions and mesh quality are the first integers to be set. Note here that an additional 5 mm will be added to the coupon length. This extra length is an extra zone at each end where no failure can occur. These zones are added to ensure that stress concentrations from the boundary conditions does not affect the result. The recommendation is to leave the mesh quality (`e1_length`) at 0.25 mm if there is no particular reason to change it. Further, some failure mechanisms are dependent on the coupon size. For that reason, try to mimic the experimental coupon as close as possible. Standard coupon sizes for different tests are seen in *Table B.1*.

Table B.1: Coupon size for different test types

	Length (mm)	Width (mm)	Hole Diameter (mm)
UNT	100	25	
UNC	13	13	
OHT	100	36	6
OHC	36	36	6
Shear	1 element	1 element	

- The next step is to decide how long the analysis will run. The default speed of the deformation (V_x) is 10 mm/s. Suggested step length is to use 100 steps/simulation but this can be altered if finer resolution is sought.
- `Laminate_rotation` allows the user to rotate the whole laminate. The rotation is defined in degrees, positive in the anticlockwise direction.
- If one of the default laminates are to be used, state laminate and environment as seen in *Figure B.2*.

```

37 # Settings Default material and layup
38 Environment='RTD' # Set environmet, valid input "RTD", "CTD" or "HTW", Give material data for T700/DT120
39 Laminate = 'B' # valid inputs: 'A', 'B' and 'C'. If user defined layup set to 'D'

```

Figure B.2: Settings for default material or layup.

- If a user defined layup is tested, three different lists have to be defined in order to get a complete layup, see *Figure B.3*. These lists contains fibre direction, thickness and material for each ply. **If a default layup are to be used, all inputs in *Figure B.3* should be commented!**

- The parameter `layup_angles` defines the layup of the laminate. There are three different kind of inputs representing UD, weave and NCF respectively. To create a UD-ply, write an integer representing its angle measured from the global x -axis. To create a weave or NCF, the input has to be a string with a letter, T or N, followed by a number representing the rotation angle as in *Figure B.3*. The T is a symbol for twill but the command is valid for any type of weave while N represents NCF. **Note that both the weave and NCF are modelled as two perpendicular UD-plyes stacked upon each other. Hence, a twill or NCF ply must be followed by a perpendicular ply of the same type.**
- `Mat_vec` assigns a material to each ply. The naming of each material is free and will be dealt with in the next step.
- The parameter `layup_thickness` defines a thickness for each ply. For the twill and the NCF, assign half of the total thickness to each ply.
- Further the input `symmetry` seen in *Figure B.3* will if set to 1 assume a symmetry line at the end of the layup lists. This means that a symmetry boundary condition will be used if loaded in tension or shear. A symmetric ply layup will be built if the load case is compression to avoid constriction of kinking.
- The last two inputs for this set are `Yt_no_insitu` and `Sl_no_insitu`. These are used to define the strength of the contact between the plies. The input should be transverse tensile strength and in-plane shear strength respectively. Both without added in-situ strength.

```

41 # Settings user defined Lay up and material. Comment this section if running default settings!!!
42 Yt_no_insitu=26.6 # This is used to define the strength of the contact, Tn=1.5*Yt_no_insitu
43 Sl_no_insitu=25 # This is used to define the strength of the contact, Ts=Tt=1.125*Sl_no_insitu
44 symmetry = 0
45 layup_angles = [T_0',T_90',T_0',T_90']
46 layup_thickness = [0.32,0.32,0.32,0.32]
47 Mat_vec = [Twill',Twill',Twill',Twill']

```

Figure B.3: Parameters to define a layup.

7. use the `Mat_paras` input to define a new material. The `Mat_paras` input can contain an unlimited number of materials. It can also contain materials that are not used in the layup. Each material in the list consists of two strings according to *Figure B.4*. The first string is the material name. The name is the id that should correspond to the ones stated in `Mat_vec`. The second string contains all material parameters in the same order as stated in section B.2. In sections B.2 to B.5 is a description of how to collect and calibrate these material parameters. The use of user defined materials are not compatible with the default materials. `Mat_paras` must therefore contain all materials used. **If a default material are to be used this row should be commented!**

```

48      Mat_paras =
      [[ 'Twill', '130000,7500,0.3,0.4,4500,1920,725,40,140,50,53,3.25,52.75,0.27,0.29,16,0.2,97.8,35.5,0.084,106.3,0.256,1.626,0.0108,0.7874,5.0012,0.01,0.7874,5.0012,0.01,1,0.32' ],
      [ 'NCF', '117000,7500,0.3,0.4,4500,1960,733,40,140,50,53,3.152,75,0.27,0.29,16,0.2,97.8,35.5,0.084,106.3,0.256,1.626,0.0108,0.7874,5.0012,0.01,0.7874,5.0012,0.01,0,0.14' ] ]

```

Figure B.4: Input for new materials.

8. Run script!

B.2 Collect material data

Material parameters in *Figure B.4* have to be collected for every new material. The material parameters needed and how to find them are described below. It is important that the material parameters in the *Abaqus* input file follows the same order as the parameters below.

Longitudinal stiffness, E_1 [MPa]

The longitudinal stiffness is taken from a physical UNT test of a UD-laminate on material level which is loaded in 0° to the fibres. Use the initial material stiffness.

Transverse stiffness, E_2 [MPa]

The transverse stiffness is taken from a physical UNT test of a UD-laminate on material level which is loaded in 90° to the fibres. Use the initial material stiffness.

Major Poisson's ratio, ν_{12}

The major Poisson's ratio is collected from a physical UNT test of a UD-laminate on material level which is loaded in 0° to the fibres.

Major transverse Poisson's ratio, ν_{23}

Use 0.4 if not measured.

In-plane shear stiffness, G_{12} [MPa]

The in-plane shear stiffness is collected from a physical shear test of a UD-laminate on material level. Use the initial material stiffness.

Longitudinal tensile strength, X_t [MPa]

The longitudinal tensile strength is taken from a physical UNT test of a UD-laminate on material level which is loaded in 0° to the fibres.

Longitudinal compressive strength, X_c [MPa]

The longitudinal compressive strength is taken from a physical UNC test of a UD-laminate on material level which is loaded in 0° to the fibres.

Transverse tensile strength, Y_t [MPa]

The transverse tensile strength is taken from a physical UNT test of a UD-laminate on material level which is loaded in 90° to the fibres.

Transverse compressive strength, Y_c [MPa]

The transverse compressive strength is taken from a physical UNC test of a UD-laminate on material level which is loaded in 90° to the fibres.

In-plane shear strength, S_{12} [MPa]

The in-plane shear strength is taken from a physical shear test of a UD-laminate on material level. Take strength at the point where nonlinearity occurs.

Fracture plane angle, α_0 [$^\circ$]

Use 53° if not measured.

Initial fibre misalignment angle, ϕ_0 [$^\circ$]

Calculate from $\phi_0 = \frac{S_{12}}{X_c}$.

Transverse shear strength, S_{13} [MPa]

Calculate from $S_{13} = \frac{Y_c}{2 \tan \alpha_0}$.

Longitudinal shear strength slope coefficient, η_L

Calculate from $\eta_L = -\frac{S_{12} \cos 2\alpha_0}{Y_c \cos^2 \alpha_0}$.

Transverse shear strength slope coefficient, η_T

Calculate from $\eta_T = -\frac{1}{\tan 2\alpha_0}$.

Transverse Young's modulus slope coefficient, η_E

Use 16 if not measured.

Shear modulus slope coefficient, η_G

Use 0.2 if not measured.

Critical energy release rate in fibre tension, G_{IC}^{FT} [mJ/mm^2]

If not measured use 97.8

Critical energy release rate of 2nd failure process in fibre tension, $G_{IC}^{FT,sec}$ [mJ/mm^2]

If not measured use 35.5

Ratio, strength over 2nd failure process in fibre tension, r^{FT}

If not measured use 0.084

Critical energy release rate in fibre kinking, G_C^{Kink} [mJ/mm^2]

If not measured use 106.3

Critical energy release rate in matrix mode I, G_{IC}^M [mJ/mm^2]

If not measured use 0.256

Critical energy release rate of 2nd failure process in matrix mode I,
 $G_{IC}^{M,sec}$ [mJ/mm²]

If not measured use 1.626

Ratio, strength over 2nd failure process in fibre tension, r_I^M

If not measured use 0.01

Critical energy release rate in matrix mode II, G_{IIC}^M [mJ/mm²]

If not measured use 0.7874

Critical energy release rate of 2nd failure process in matrix mode II,
 $G_{IIC}^{M,sec}$ [mJ/mm²]

If not measured use 5.0012

Ratio, strength over 2nd failure process in fibre tension, r_{II}^M

If not measured use 0.01

Critical energy release rate in matrix mode III, G_{IIIC}^M [mJ/mm²]

If not measured use 0.7874

Critical energy release rate of 2nd failure process in matrix mode III,
 $G_{IIIC}^{M,sec}$ [mJ/mm²]

If not measured use 5.0012

Ratio, strength over 2nd failure process in fibre tension, r_{III}^M

If not measured use 0.01

Flag for bilinear or trilinear damage law, flaglawmat

For weave use 1, else use 0.

Ply thickness, pthick

Thickness of the ply.

B.3 Calibrate collected material data

When all material parameters are collected some of them needs to be calibrated on material level. Follow the procedure below to calibrate the material parameters for a UD-ply.

1. Make a virtual shear test on a $[0/90]_n$ UD-laminate at material level. Calibrate the in-plane shear strength, S_{12} , such that the failure stress in the virtual test correlate to the first indication of failure in the physical tests.
2. Make a transverse virtual tensile test on a UD-laminate at material level. Calibrate the transverse tensile strength, Y_t and the transverse stiffness E_2 until the failure strength and strain are similar to the ones of the physical tests.
3. Make a longitudinal virtual tensile test on a UD-laminate at material level. Calibrate the longitudinal stiffness E_1 and the longitudinal tensile strength X_t until the failure stress and strain matches the ones of the physical tests.
4. Make a longitudinal virtual compression test on a UD-laminate at material level. Calibrate the initial fibre misalignment angle ϕ_0 such that the failure stresses are similar in the virtual and physical tests.

If there is a twill or NCF involved in your laminate, adjust the calibrated UD-properties so that they can be used for twill and NCF modelling. Use a physical test of a twill/NCF with layup $[0/90]$ and follow the two calibration steps below. The procedure is the same for both twill and NCF.

1. Perform a virtual tension test of a twill/NCF with layup $[0/90]$ and load in 0° . Reduce the longitudinal stiffness and strength to obtain a similar failure strength and strain as in the physical tests.
2. Perform a virtual compression test of a twill/NCF with layup $[0/90]$ and load in 0° . Increase the fibre misalignment angle to obtain a similar failure strength and strain as in the physical tests.

B.4 In-situ strength

Apply in-situ theory and increase transverse tensile strength, in-plane shear strength and transverse shear strength for UD-plyes. The in-situ strengths are calculated using the file `In-situ_Template.xlsm`.

B.5 Different environments

When testing materials in other environments than RTD, redo sections B.1 and B.2 with some differences when collecting the material data. These differences are mentioned below.

1. The longitudinal and transverse stiffness are collected from physical UNC tests instead of UNT tests. Use tests of a UD-laminate on material level which is loaded in 0° and 90° towards the fibres.
2. Use the same major Poisson's ratio ν_{12} and longitudinal tensile strength X_t as in RTD.
3. Calculate the transverse tensile strength, Y_t , from the following equation where superscript *RTD* represents the room temperature environment.

$$Y_t = Y_t^{RTD} \frac{E_2}{E_2^{RTD}}$$

All other parameters are collected in the same way as for RTD. The calibration part in section B.3 is partly changed and reads as below.

1. Make a virtual shear test on a $[0/90]_n$ UD-laminate at material level. Calibrate the in-plane shear strength, S_{12} , such that the failure stress in the virtual test correlate to the first indication of failure in the physical tests.
2. Make a transverse virtual compression test on a UD-laminate at material level. Calibrate the transverse shear strength, S_{13} , so that the failure strength is the same in the virtual and physical tests. Also calibrate the transverse stiffness, E_2 , such that the virtual and physical tests have the same initial stiffness.
3. Make a longitudinal virtual compression test on a UD-laminate at material level. Calibrate the initial fibre misalignment angle ϕ_0 such that the failure stress is equal in the virtual and physical tests. Also calibrate the longitudinal stiffness, E_1 , such that the virtual and physical tests have the same initial stiffness.

If there is a twill or NCF involved in your laminate, adjust the calibrated UD-properties so that they can be used for twill and NCF modelling. This is done by reducing the longitudinal stiffness and strength by the same factors as they were reduced by in RTD environment. Also increase the initial misalignment angle, ϕ_0 , by the same factor as it was increased by in RTD environment. Finally, use in-situ strength in the same way as in RTD environment, see section B.4.

C Stress-strain charts for all unnotched laminate tests

